BACCHUS

Impact of Biogenic versus Anthropogenic emissions on Clouds and Climate: towards a Holistic UnderStanding

Collaborative Project

SEVENTH FRAMEWORK PROGRAMME
ENV.2013.6.1-2

Atmospheric processes, eco-systems and climate change

Grant agreement no: 603445

Deliverable number:	**D4.3**
Deliverable name:	Estimates of aerosol climate forcing
WP number:	4
Delivery date:	Project month 36 (30/11/2016)
Actual date of submission:	01/12/2016
Dissemination level:	PU
Lead beneficiary:	MPG
Responsible scientist/administrator:	Stefan Kinne and Bjorn Stevens
Estimated effort (PM):	40 PM
Contributor(s):	Stefan Kinne, Bjorn Stevens (MPG), David Neubauer (ETHZ)
Estimated effort contributor(s) (PM):	MPG: 34 PM, ETHZ: 6 PM
Internal reviewer:	Ulrike Lohmann

Task 4.3: Aerosol climate forcing

Executive summary: An aerosol climatology for aerosol optical properties (including estimates for associated CCN and CDNC) has been developed involving observation statistics from ground based remote sensing in a (from optics to microphysics, thus) top-down approach two aerosol monthly climatologies were developed: **M**ax-Planck **A**erosol **C**limatology in its second version (MACv2) and its twin MACv2-SP. While the properties and assumptions for both climatologies are outlined in Appendices A and B, the focus is on associated estimates for the combined direct and indirect radiative forcing by anthropogenic aerosol (TOA, all-sky). MACv2 is applied in off-line radiative transfer modeling and results for direct and indirect aerosol forcing and aerosol radiative effects are presented. For current conditions the clear-sky radiative forcing is at -0.5 W/m^2, which is reduced by the actual presence of clouds to -0.2 W/m^2 (all-sky). The local variability is larger by up to one order of magnitude of both signs. The (first) indirect TOA forcing is negative everywhere and on average almost four times more negative than the direct effect. The combined TOA forcing of about -1.0 W/m^2 in 'climate cooling' has not changed much over the last 30 years - despite major shifts in 'cooling' maxima away from the EU (and the US) to SE-Asia (and even western Africa). Surface net-flux losses and atmospheric solar heating are dominated, in contrast to the TOA, by direct aerosol effects.

In parallel, MACv2's simpler twin, MACv2-SP (Single Plume), was developed. Central elements of MACv2-SP are (1) the representation of global maps for the current anthropogenic AOD by a set of regional plumes and (2) the use of a statistical relationship that links anthropogenic fine-mode AOD directly to CDNC changes. MACv2-SP (Single Plume) approximates the anthropogenic AOD map of MACv2 by distribution patterns of nine (5 pollution and 4 wildfire) sources and also applies a simple and surprisingly well performing AODf vs CDNC relationship to prescribe the aerosol impact on water clouds. Despite its simplicity, the resulting indirect forcing pattern closely matches the indirect forcing pattern of a much more elaborate (via CCN) approach. Still when applied in the ECHAM climate model the resulting indirect forcing is about half as large as in the MACv2 environment, while estimates for direct (clear-sky and all-sky) forcings are similar. MACv2-SP will define anthropogenic aerosol and its simple link CDNC change will also test the response of cloud schemes in upcoming RFMIP simulation exercises (as part of CMIP6). MACv2-SP will provide harmonized aerosol input in RFMIP simulations and its link to CDNC changes will be an interesting challenge for various cloud schemes.

Introduction

Most estimates for aerosol climate effects are so called bottom-up approaches. In those approaches emission data of particles and pre-cursor gases are assigned and then model processed (e.g. chemistry, transport, removal) which yields 3D mass distributions. The mass distributions are then converted (with additional assumptions to aerosol size and water uptake) to yield aerosol optical properties. Hereby, the model simulated optical properties are usually stratified into the two (optically active) size-modes: the fine-mode (representing all particles with radii between 0.05 and 0.5µm) and the coarse-mode (representing all aerosol particles with radii larger than 0.5µm). Only at this stage (optical property model output) of bottom-up modeling, a comparison to local quality observations (by sun-/sky-photometry) is possible. Major differences to these reference data are then used to review and if necessary adjust processes or assumptions. The identification of shortcomings with processes in modeling and finding better, preferably simpler and observationally constrained approaches is a goal of past and ongoing AeroCom experiments. Once the aerosol optical properties are in a reasonable good shape, then they are applied in broadband radiative transfer schemes to yield aerosol associated radiative effects and aerosol forcing.

An alternate top-down approach starts with observational data for all relevant aerosol optical properties as they are offered by sun-/sky-photometry from the ground. And these observations offer a direct link to associated aerosol radiative effects via radiative transfer interpretations. Unfortunately, these observations are spatially sparse and information on the spatial context is required to yield the needed complete global fields. Since the climatology approach relies on multi-annual monthly observational averages of all relevant aerosol properties (number concentrations, composition and size), an ensemble average of bottom-up modeling is picked to provide the spatial context. Note, that satellite data, as commonly used in aerosol data assimilations, are not an option, because they are also spatially sparse and because they address with limited accuracy usually only one aerosol property. The merging of monthly statistics between observations and modeling is done such that each aerosol property distribution from modeling is individually increased or decreased depending on the observation-to-model (interquartile average) ratios at common points. These adjustments are done individually over sub-regions with sufficient observational reference data. The resulting adjusted global fields are termed MACv2 aerosol climatology (see Appendix A) and, based on this, its simplified twin MACv2-SP has been developed (see Appendix B) for harmonized aerosol impact experiments in RFMIP.

The content of the deliverable addresses aerosol radiative impacts in this order:

- direct aerosol radiative effects and forcing with MACv2 (current)
- (first) indirect aerosol radiative forcing with MACv2 (current)
- direct vs indirect aerosol radiative effects with MACv2 (current)
- time slices for aerosol (TOA) forcing with MACv2 (e.g. year 2005 vs year 1985)
- radiative forcing with MACv2-SP in ECHAM
- temporal forcing change aspects

Direct aerosol effects and forcing - currently

The MACv2 aerosol climatology is applied in an off-line radiative transfer model to determine today's aerosol direct impacts on radiative net-flux changes at top of the atmosphere (TOA) and at the surface. Annual average maps are presented in Figure 1 for the (1) combined solar and infrared impact of total aerosol, (2) solar only effects of total aerosol and (3) anthropogenic (solar) impacts. Results are given for both clear-sky conditions and with ISSCP cloud statistics. The climate relevant radiative TOA effect at all-sky conditions, termed `aerosol direct forcing' is relatively small and has been multiplied by a factor of 10 for better visibility in Figure 1. For more detail on aerosol direct forcing, its monthly averages are presented in Figure 2.

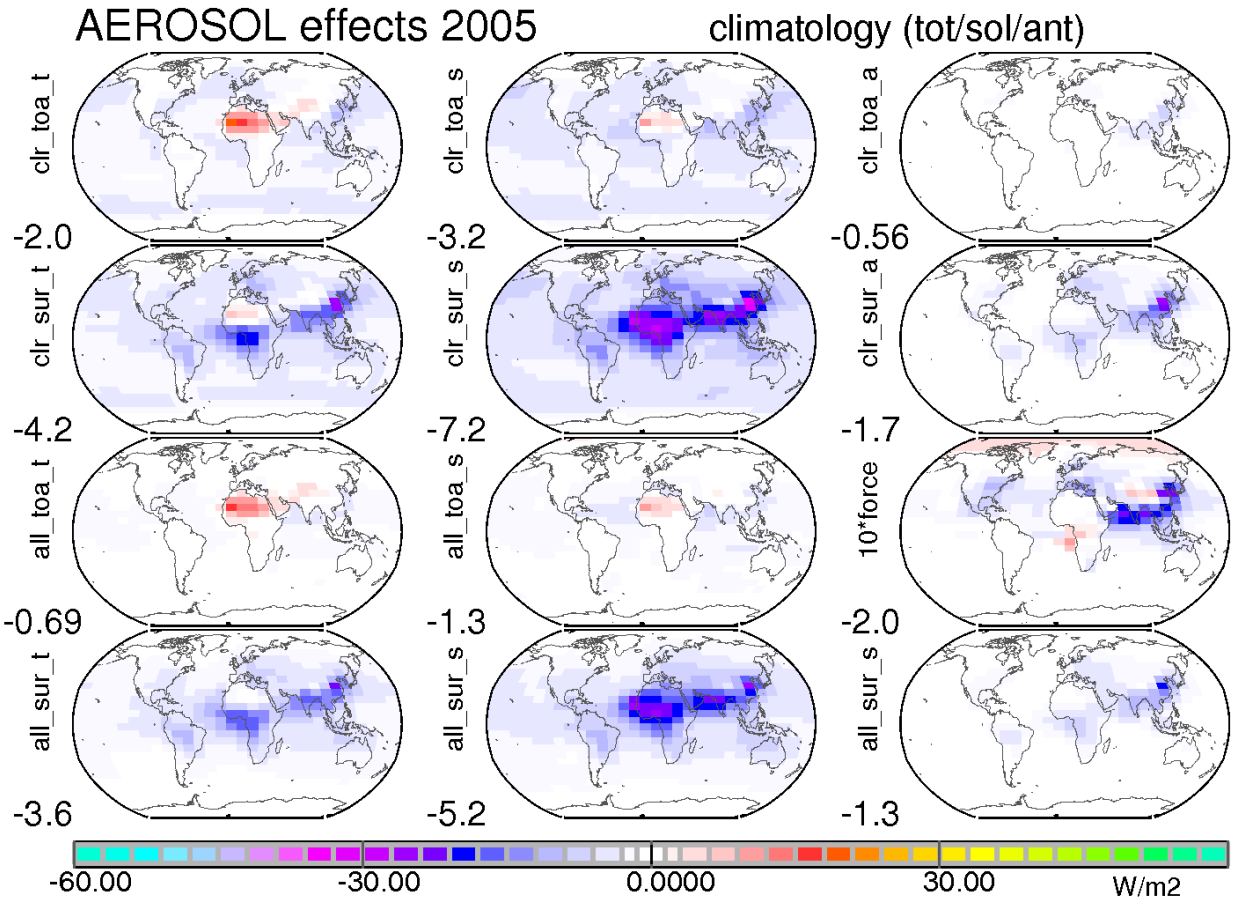

Figure 1: Overview of direct radiative effects of today's tropospheric aerosol by applying the MACv2 aerosol climatology. The top two rows give spatial distributions of the aerosol radiative effects at cloud free conditions. The bottom two rows include ISCCP cloud statistics in the simulations to represent all-sky conditions. Rows 1 and 3 display the effects on radiative net-fluxes at TOA, while rows 2 and 4 show the effects on radiative net-fluxes at the surface. Compared are today's total aerosol effects (column 1), today's total solar only effects (column 2) and today's anthropogenic aerosol effects (column 3). The 3rd panel in the 3rd row represents the direct forcing (TOA, all-sky) for today's anthropogenic aerosol. Since it is small compared to all other presented aerosol effects it has been multiplied by a factor of 10 for better visibility. Values below labels show global averages (thus, the annual global direct forcing is at -0.2W/m^2).

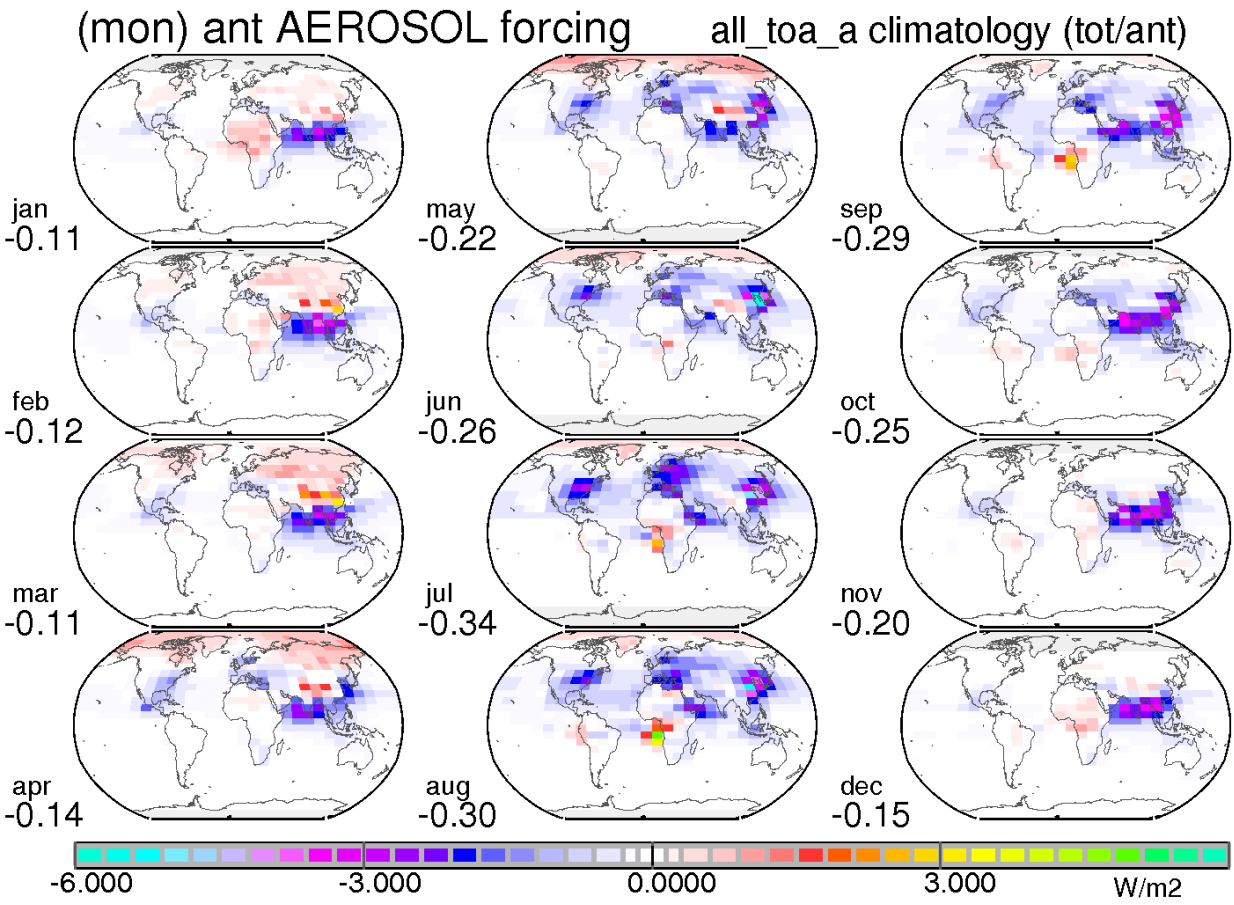

Figure 2: Spatial distributions for the monthly direct radiative TOA forcing by today's ('year 2005') anthropogenic aerosol. A negative value indicates 'climate cooling', while a positive value indicates 'climate warming'. Global monthly averages for each month are indicated below each label.

The global average direct aerosol radiative forcing is -0.2 W/m^2. There is significant regional and seasonal variability with values up to an order of magnitude larger of both signs. Globally the direct aerosol forcing is smallest during the boreal winter (-0.11 W/m^2) and largest during the boreal summer (-0.34 W/m^2). Strongest positive forcing is caused by absorbing aerosol that dims the brightness of lower altitude clouds: over the SE Atlantic in August and September and over China in February and March. Positive forcing also occurs over snow covered ground. Strongest negative forcing (related with larger pollution) occurs over China from June to September and over India from September to March. Over the last decades (as will be shown later) the overall direct aerosol cooling has decreased as the anthropogenic aerosol composition has become more absorbing (overall less from non-absorbing components: much less sulfate, although more nitrate and overall more absorbing components: more soot).

(First) indirect aerosol forcing - currently

Monthly averages for the (first) indirect radiative forcing of the MACv2 climatology are presented in Figure 3. There are many assumptions involved and it was postulated that the by anthropogenic aerosol increased cloud water cloud droplet concentrations translate into increases to cloud optical depth, thus also increases in planetary albedo. Only this single ('Twomey') indirect impact is considered, postulating that cloud lifetime changes are less important also due to partially cancellation (e.g. easier evaporation vs precipitation delay). Also assumed is a super-saturation of 0.1% and a logarithmic relationship between anthropogenic aerosol assigned active nuclei (CCN) and cloud droplets (CDNC). On average the TOA net-fluxes are strongest reduced over oceanic low cloud regions especially during times with extended sun-light times with intermediate sun-elevations (e.g. mid-latitude summers). The impact applies MACv2 associated CCN data (see Appendix A) and assumes that resulting CDNC changes (which also depend on the local CCN background) translate into increases for the planetary albedo (assuming that the cloud water content does not change). Note, spatial forcing patterns are more important, since indirect forcing strength depends on the CCN pre-factor choice for the logarithmic relationship between CCN and CDNC.

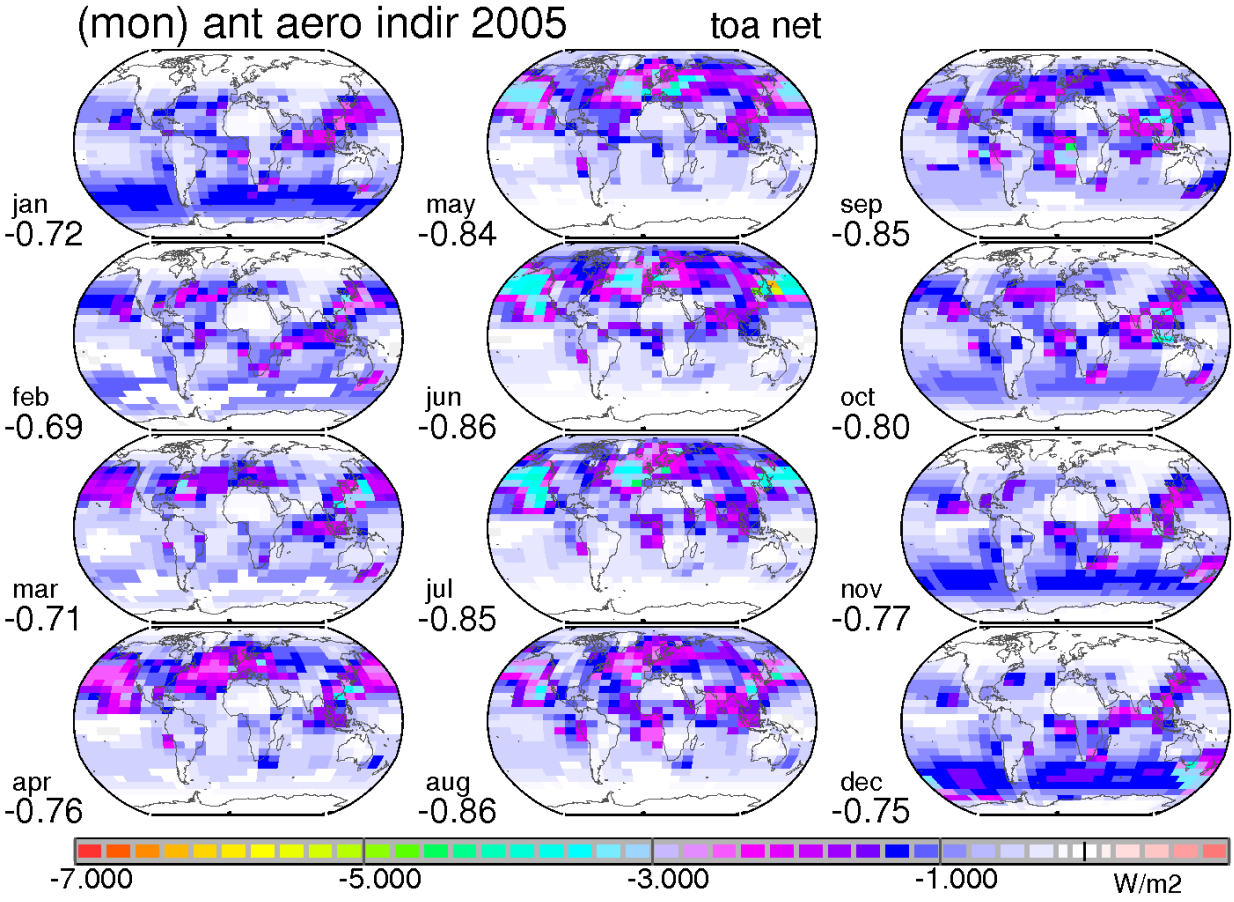

Figure 3: Tropospheric monthly indirect radiative forcing by today's ('year 2005') anthropogenic aerosol.

Direct vs indirect effects - currently

In this sub-chapter spatial patterns and strengths between clear-sky, direct all-sky and (first) indirect radiative effects of today's anthropogenic aerosol attributed by the MACv2 aerosol climatology are compared to each other - also in context of the total (direct all-sky and indirect) radiative effects. Annual average radiative effects for TOA net-fluxes are compared in Figure 4, atmospheric impacts are shown in Figure 5 and surface net-flux impacts are given in Figure 6. At the TOA the radiative impact is dominated by the indirect effect although the direct effect introduces spatial variability. Interestingly, direct 'warming' at all-sky conditions (introduced by considering clouds) is more than compensated by indirect 'cooling (Figure 4).

Introducing clouds reduces the clear-sky TOA forcing, while indirect cloud albedo increases the aerosol radiative forcing to more negative values. For simplified total forcing approximations was hoped that due to cloud compensating effects the total aerosol forcing could be represented by clear-sky forcing, but the patterns differ.

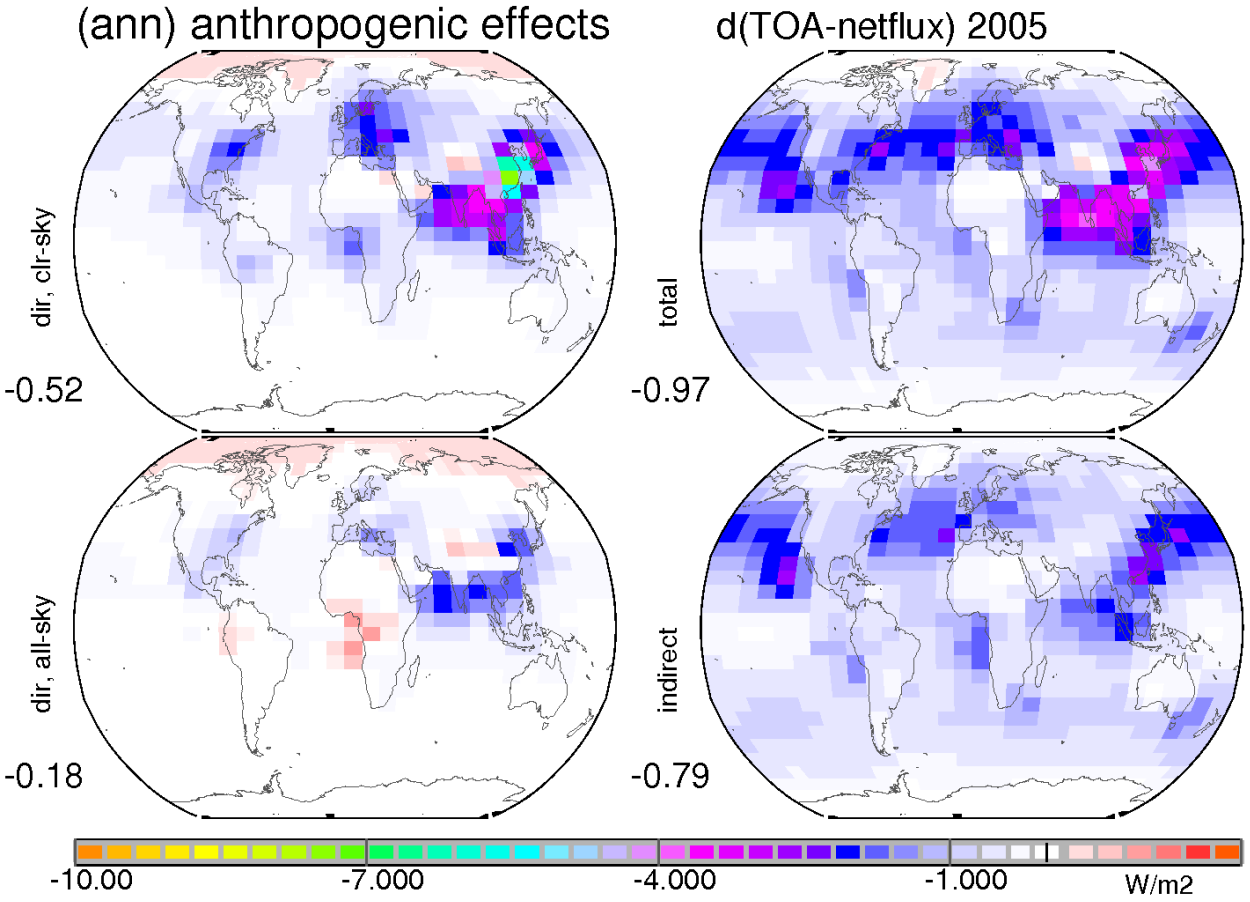

Figure 4: Annual radiative TOA net-flux changes by today's ('year 2005') anthropogenic aerosol. Presented are spatial distributions of (1) clear-sky radiative effects (upper left panel), (2) direct effects with ISSCP clouds (lower left panel), (3) indirect effects (from aerosol reduced water cloud drop sizes, upper right panel) and (4) the total impact (lower right panel).

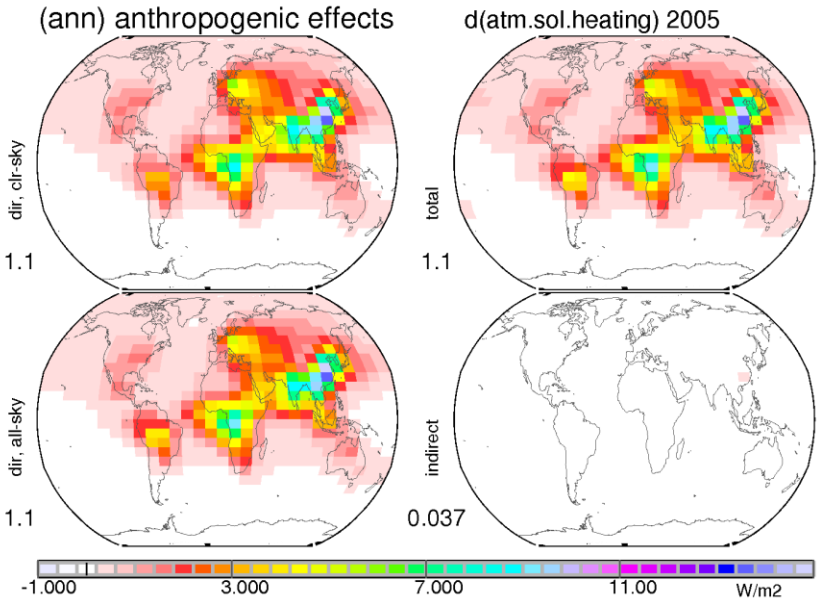

Figure 5: Annual solar heating rate changes by today's ('year 2005') anthropogenic aerosol. Presented are spatial distributions of (1) clear-sky radiative effects (upper left panel), (2) direct effects with ISSCP clouds (lower left panel), (3) indirect effects (from aerosol reduced water cloud drop sizes, upper right panel) and (4) the total impact (lower right panel).

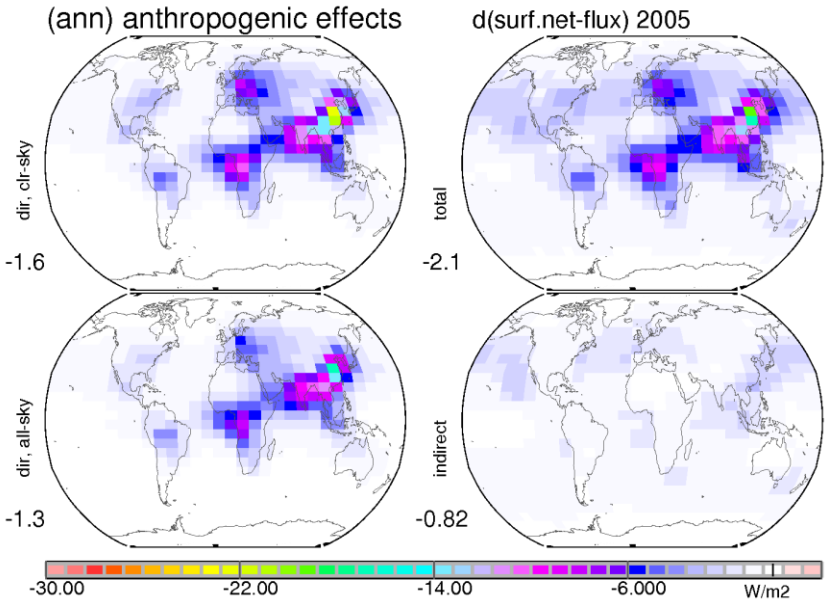

Figure 6: Annual radiative net-flux changes at the surface by today's ('year 2005') anthropogenic aerosol. Presented are spatial distributions of (1) clear-sky radiative effects (upper left panel), (2) direct effects with ISSCP clouds (lower left panel), (3) indirect effects (from aerosol reduced water cloud drop sizes, upper right panel) and (4) the total impact (lower right panel).

Time slices for aerosol (TOA) forcing

With temporal changes to anthropogenic AOD through scaling (using bottom-up transient ECHAM simulations for historic times and using predicted emission scenarios for sulfate (RCP 8.5) of bottom-up simulation for future times) MACv2 can offer aerosol maps for the entire 1850 to 2100 period. Here, anthropogenic forcings (direct all-sky, indirect and combined total) are compared between 1965, 1985, 2005 and 2025 (Figure 7). More detailed comparisons only between 1985 and 2005 are presented in Figures 8 (TOA), 9 (atmosphere) and 10 (surface).

The total aerosol forcing currently has reached its maximum at just below -1W/m² globally. The direct (and possibly also indirect effects) will slightly increase, when considering the more scattering anthropogenic aerosol type of the past. Thus, ***the total aerosol forcing has stayed pretty constant since the 1980ies*** despite pollution center shifts and compositional change.

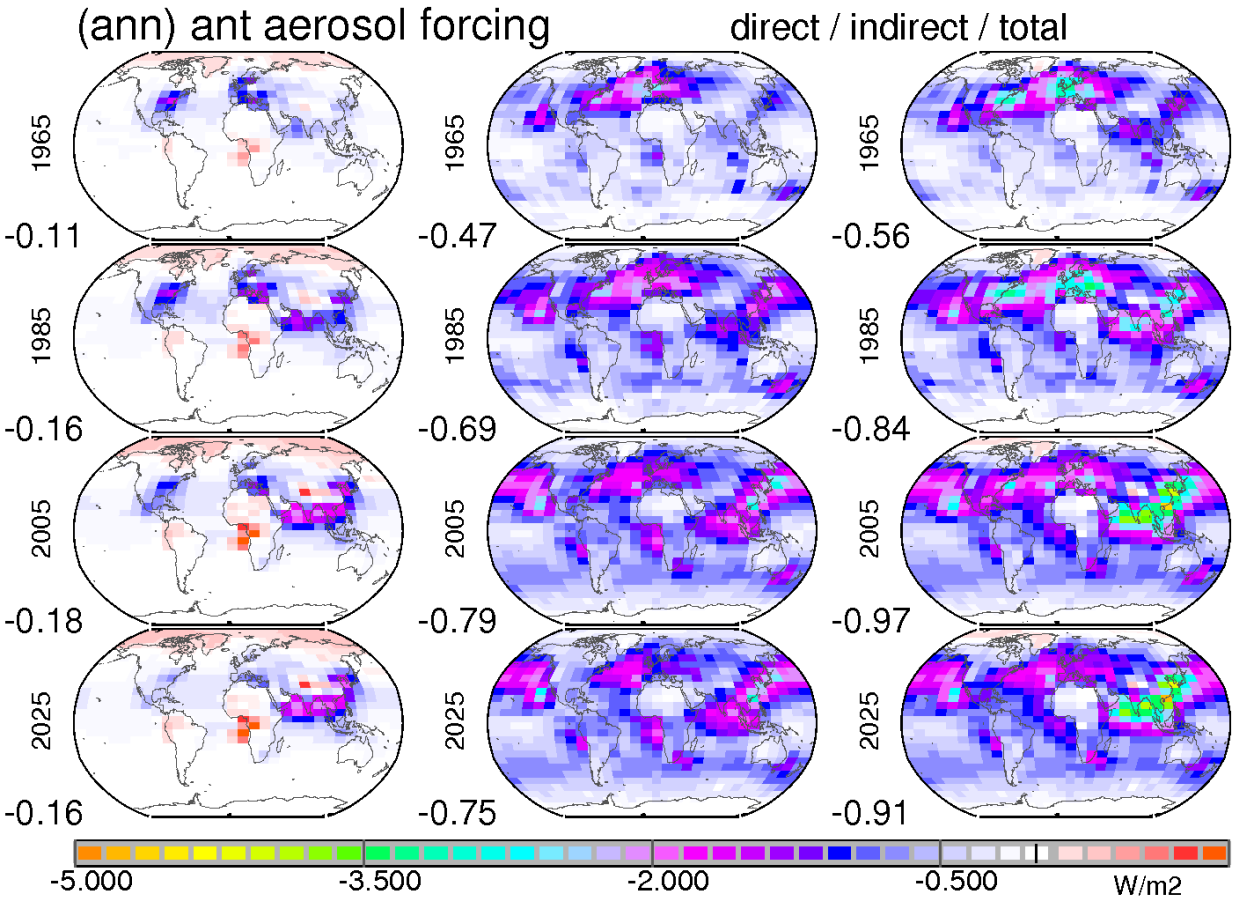

Figure 7: Annual slices (years 1965, 1985, 2005 and 2025) of anthropogenic aerosol forcing spatial distributions for direct effect (column 1), indirect effects (column 2) and combined total (column 3). Note that the composition (e.g. absorption) of anthropogenic aerosol here was not allowed to vary over time. This will yield increasing larger direct effects back to the 1980ies, so that on a global annual average the aerosol climate impact (TOA, all-sky) over the last 30 years remained almost unchanged at ca -1W/m².

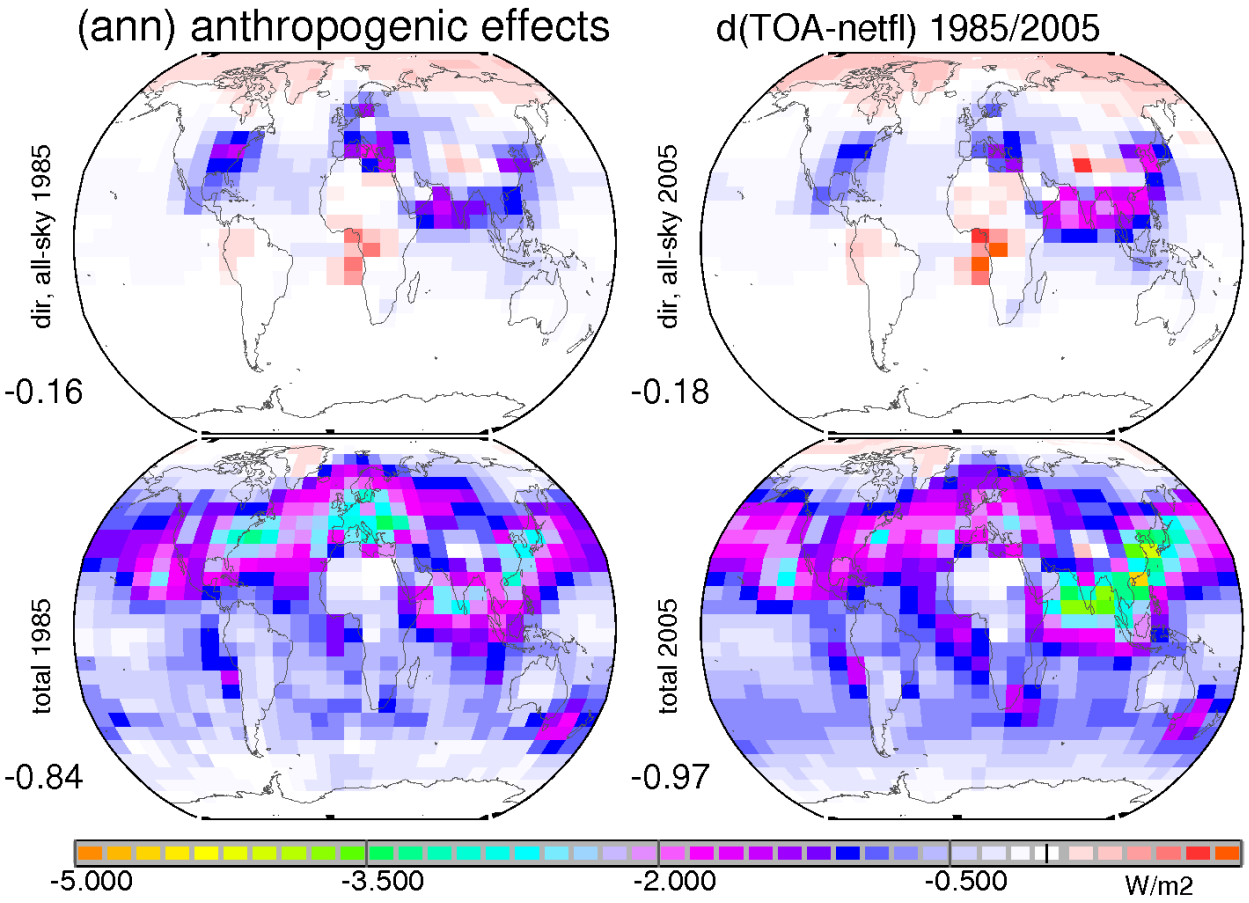

Figure 8: A comparison of annual radiative TOA net-flux changes by anthropogenic aerosol comparing years 1985 (left column) and 2005 (right column),. Presented are spatial distributions of (1) direct effects with ISSCP clouds (all-sky, upper row) and (2) total (direct and indirect) impacts (lower row)..

At the TOA the anthropogenic impact is dominated by the indirect effect, whereas for atmospheric and effects on net-fluxes the anthropogenic direct effect is more influential.

For the TOA effects between 1985 and 2005 when pollution shifted from US/EU to SE Asia there were strong regional shifts as cooling maxima shifted from mainly Europe to SE-Asia. Still, changes to the TOA global average forcing are small. For atmospheric effects a global increase of the atmospheric solar heating by about 20% was found. This increase is probably even larger considering a more absorbing aerosol type in 2005 (see below). The atmospheric solar heating over SE Asia has approximately doubled from 1985 to 2005 and also increases over western central Africa and South America are significant.

Similarly, to atmospheric absorption increases also the reductions to the surface net-fluxes have increased between 1985 and 2005, even with smaller contributions from the indirect effect. We did not consider that in the past (1950-1990) anthropogenic aerosol was likely less absorbing which mainly would have led to a more negative direct effect – so the overall aerosol cooling in 1985 would have been similar to today at -1W/m^2. Note that direct effects dominate for the atmospheric solar heating effects (Figure 9), because of the absorption of fine (anthropogenic) aerosol particles. For radiative effects at the surface (Figure 10), direct effects dominate. Here aerosol amount and aerosol absorption matter most.

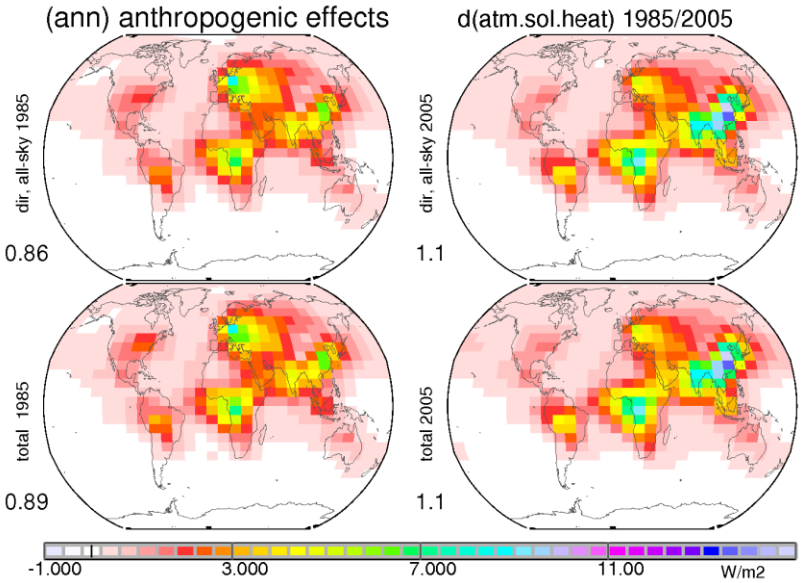

Figure 9: A comparison of annual radiative atmospheric solar heating by anthropogenic aerosol comparing years 1985 (left column) and 2005 (right column). Presented are spatial distributions of (1) direct effects with ISSCP clouds (all-sky, upper row) and (2) total (direct and indirect) impacts (lower row).

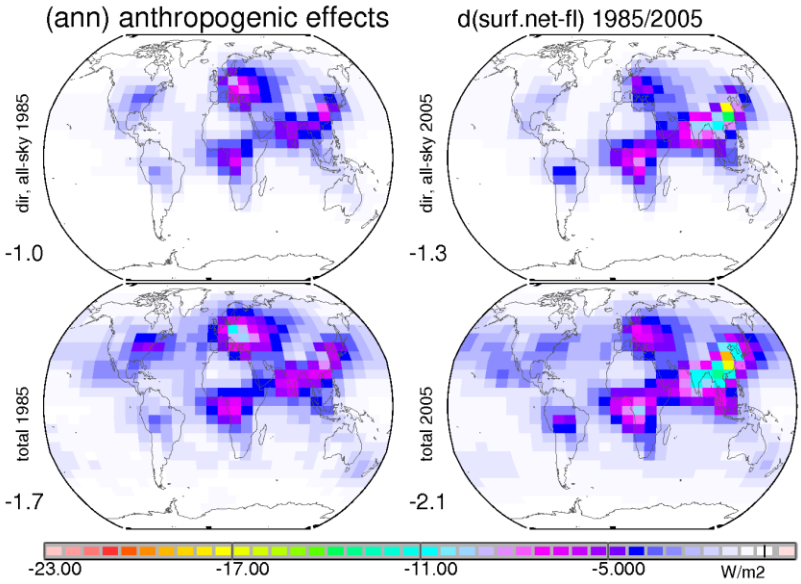

Figure 10: a comparison of annual radiative net-flux changes at the surface by anthropogenic aerosol comparing years 1985 (left column) and 2005 (right column), as in-between that time pollution shifted from US/EU to SE Asia. Presented are spatial distributions of (1) direct effects with ISSCP clouds (all-sky, upper row) and (2) total (direct and indirect) impacts (lower row).

Aerosol radiative forcing with MACv2-SP in ECHAM

The simplified MACv2-SP approach was implemented in the ECHAM global model in order to simulate the aerosol forcing for today's (2005) anthropogenic aerosol loads. Results for the effective radiative forcing (after internal model adjustments) are presented in Figure 11.

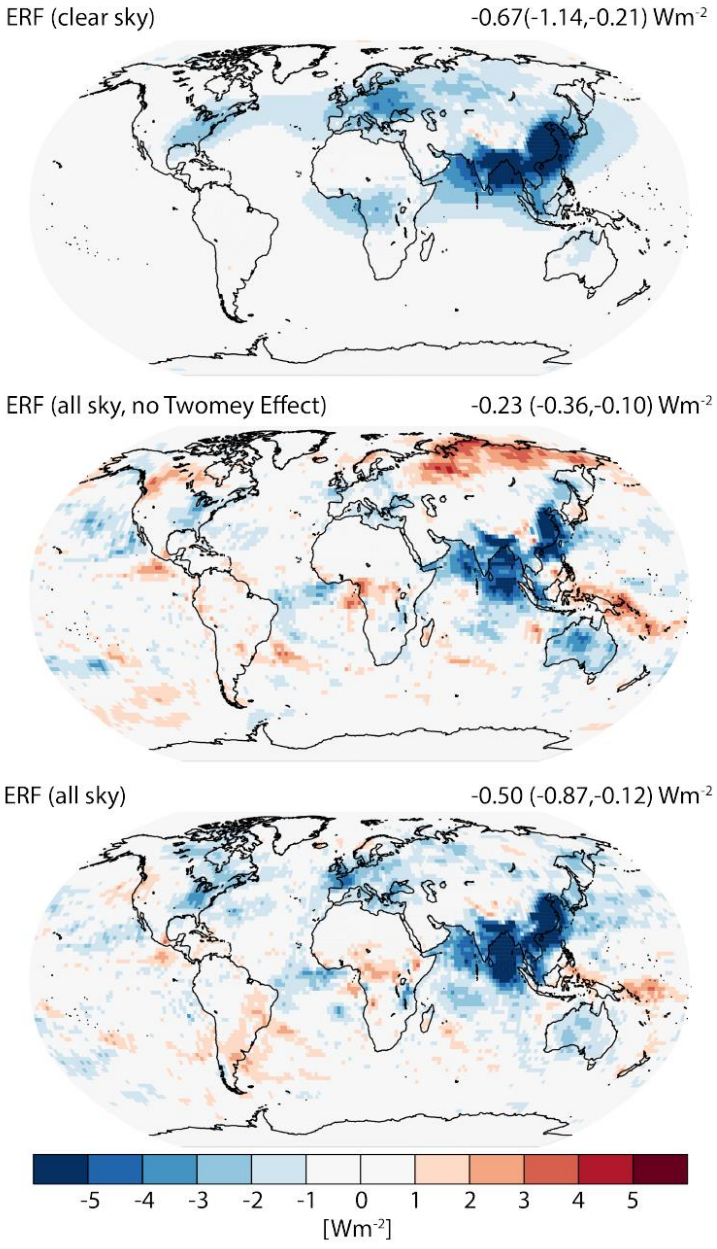

Figure 11 TOA radiative forcing by applying MACv2-SP in the ECHAM global circulation model. Results of a 10-year simulation are illustrated. Presented are annual averages for today's (2005) anthropogenic aerosol impacts for the clear-sky (effective) radiative forcing (upper panel), for the all-sky effect without the Twomey effect (center panel) and for the total (direct plus indirect) aerosol forcing (lower panel).

In Figure 11 global annual averages (with hemispheric averages in brackets) are provided for clear-sky forcing (-0.67 W/m^2), all-sky forcing (-0.23 W/m^2) and total forcing (-0.50 W/m^2). The direct forcings compare quite well to the MACv2 estimates (of -0.52 W/m^2 for clear-sky and -0.20 W/m^2 for all-sky). The indirect (total minus direct) forcing (of -0.44 W/m^2) is smaller than the MACv2 estimate (of -0.79 W/m^2). This is a bit surprising as the simplified fit yielded even a larger indirect forcing (of -0.87 W/m^2, see Appendix B). It is not quite clear why the indirect effect is so much lower. Possible candidates are (1) different water cloud distributions (e.g. differences in indirect forcing pattern) and (2) the poorly defined pre-industrial background, which (aside from the combined anthropogenic and pre-industrial fine-mode AOD) is required for the applied AODf vs CDNC relationship. Another possible argument is that ECHAM output presents an effective and not an instantaneous forcing. However, in the context of (demonstrated spatial) variability - most likely due to the varying properties of clouds in the climate model – the difference between effective and radiative forcing is probably too noisy to be significant (Figure 12).

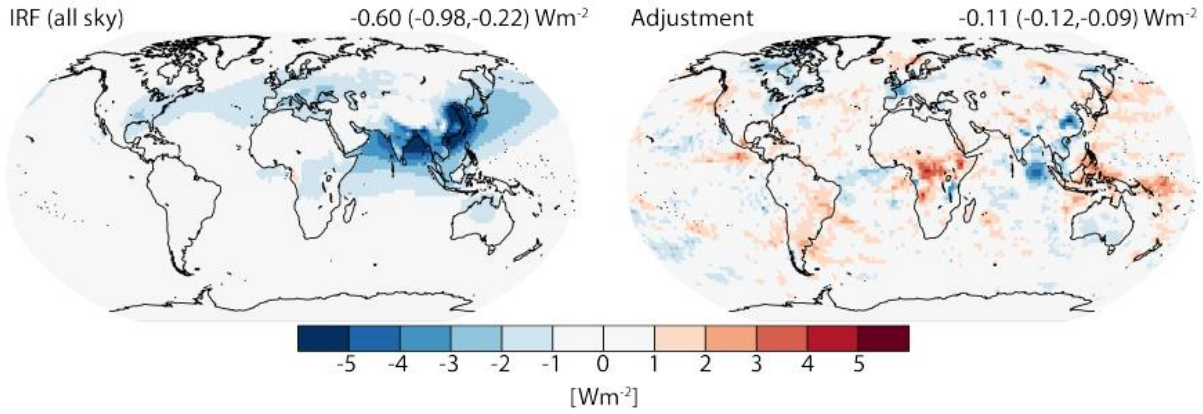

Figure 12 Annual maps for the instantaneous total (direct plus indirect) aerosol TOA forcing (left panel) and difference to the effective total aerosol radiative forcing right panel). The effective radiative forcing (involving feedback in modeling) is slightly smaller.

Temporal forcing change aspects

Recently, S. Smith (private communication) released updated historic emission data, which indicate that over time not only (local/regional) anthropogenic aerosol AOD was/is changing over time but also its absorption strength. Figure 13 illustrates the changing absorption potential of anthropogenic aerosol. Figure 13 displays that the aerosol 'cooling' potential to counteract greenhouse gas warming was stronger in the 20th century, although (not aerosol direct but) aerosol indirect effects (via cloud-modifications, if we believe MACv2) contribute stronger on average to TOA forcing. It indicates that anthropogenic aerosol was much more absorbing at preindustrial times and also has become in recent decades more absorbing. However, a more absorbing anthropogenic aerosol also means a stronger solar heating in the atmosphere. This may not only have impacts on atmospheric dynamics but may also have on aerosol indirect effects, likely causing a reduced indirect effect due to a less favorable CCN composition and enhancements for cloud drop evaporations. This compositional change has already been investigated and analyzed by G. Myhre in a recent ACP paper (Myhre et al., 2016), when inserting most recent aerosol emission data in bottom-up modeling. Their ensemble results for total aerosol forcing in Figure 14 demonstrate the strong regional shift in radiative forcing from US and Europe to SE-Asia. Future radiative forcing simulations (for impacts at TOA) and in particular comparisons of time-slices need to consider not just the anthropogenic AOD change but they also need to consider changes in aerosol compositions.

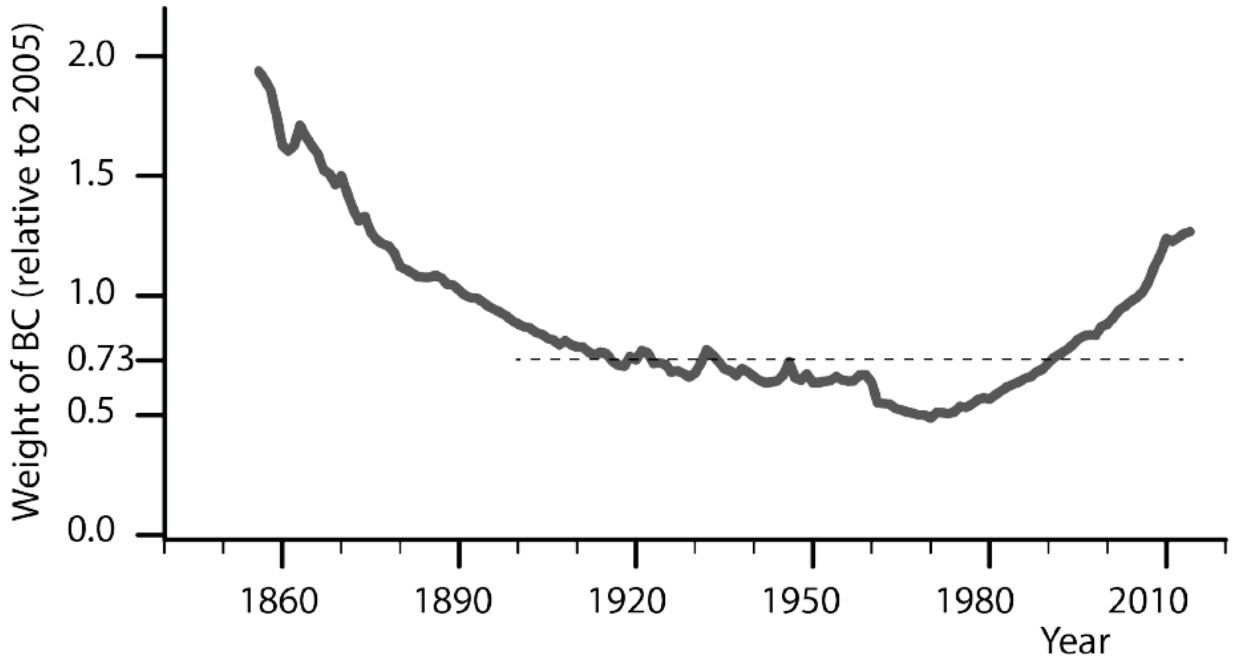

Figure 13 Relative weights in historic emission between soot and sulfate with respect to the ratio at 2005 based on historic emission data (from S. Smith).

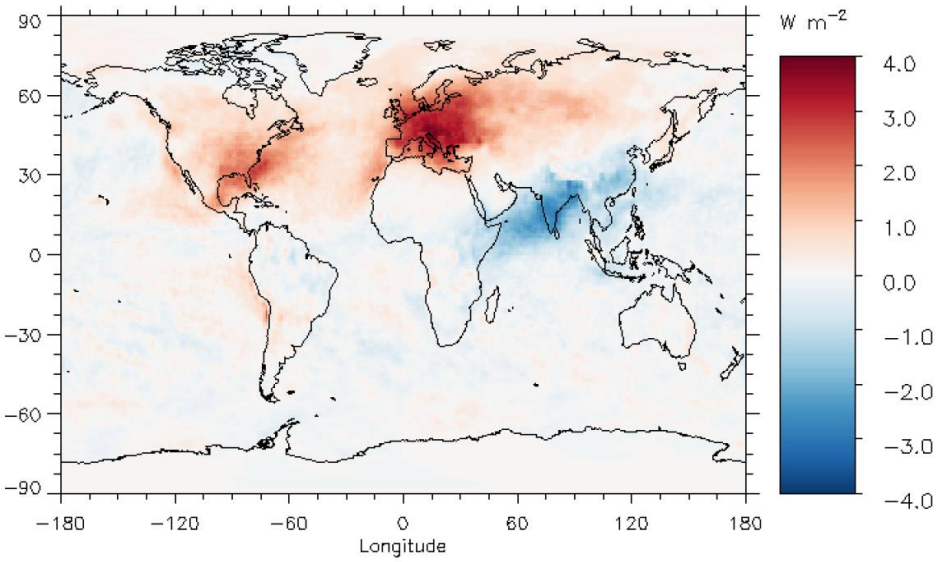

Figure 14 Regional shifts in total (direct and indirect) aerosol forcing (all-sky TOA) from an ensemble average from bottom-up modeling for year 2015 with respect to year 1990 (from Myhre et al, 2016).

Summary of results

Involving observation statistics from ground based remote sensing in a (from optics to microphysics, thus) top-down approach two aerosol monthly climatologies were developed: MACv2 and its twin MACv2-SP. The radiative forcing for current conditions is close to -1.0 W/m^2 (-0.8 W/m^2 indirect and -0.2 W/m^2 direct) and has not changed significantly over the last 30 years. For simpler MACv2-SP (9 Single Plumes approximate MACv2's anthropogenic AOD map) a simple and surprisingly well performing AODf vs CDNC satellite-sensor data based relationship is applied to prescribe the aerosol impact on water clouds. MACv2-SP will provide harmonized aerosol input in RFMIP simulations.

References

Kinne, S. et al.: MACv1: A new global aerosol climatology for climate studies (JAMES, 5 704-740, 2013)

Myhre, G. et al: Multi-model simulations of aerosol and ozone radiative forcing for the period 1995-2005 (ACPD, doi:10.5194/acp-2016-594, 2016)

Stevens, B. et al, MACv2-SP: A parameterization of anthropogenic aerosol optical properties and an associated Twomey effect for use in CMIP 6 (submitted, 2016)

Changes with respect to the DoW

None

Dissemination and uptake

MACv2 will be provided to the climate modeling community.

Appendix A **Properties of MACv2**

The Max-Planck Aerosol Climatology MACv2 is now in its second version. The update over MACv1 (Kinne et al., 2013) now also includes aerosol observations over oceans (of the Marine Aerosol Network MAN), the pre-industrial background for 1850 is raised, yielding on average a approx. 30% lower anthropogenic AOD and the merging of observations with modeling gives now a stronger weight to observations, which mainly resulted in a stronger aerosol absorption. Also a merging of relative aerosol properties (such as Angstrom, fine-mode AOD550 fraction or SSA) is avoided in this version. Instead only absolute properties (AOD 440, AOD 870, coarse-mode AOD550, fine-mode AOD550 and AAOD) are merged and then from the merged absolute properties the relative properties are determined. Moreover, the absorption, described by the absorption AOD (AAOD =AOD*[1-SSA]), is now separated into contributions by fine-mode AAOD and by coarse-mode AAOD. This opens a path to address component AOD values, that is: sulfate (SU), organic matter (OC) and soot BC of the fine-mode and sea-salt (SS) and dust (DU) of the coarse mode. This component separation simplifies the derivation of spectral properties which are needed for broadband radiative transfer simulations.

MACv2 is based on merging of monthly statistics of trusted observations onto background data (from ensemble bottom-up modeling) of all relevant aerosol (mid-visible) properties in order to address aerosol amount, composition and size. Annual averages of the local observations, of the background data and of the resulting merged fields are displayed in Figure A1 for four important aerosol column properties (AOD, AAOD, FMF and Angstrom). For the aerosol amount (AOD550) the global average of the merged data did not change much from the background but there were regional shifts, such as less AOD over Europe (where models overestimated emissions) and more over SE Asia (where models underestimated emissions). The merged results present a on average by 60% stronger absorption than the background everywhere (hereby the lack of stronger absorption for Europe not revealed as AOD is overestimated there). Aerosol size is represented by the AOD spectral dependence (Angstrom) and by the AOD fractions assigned to the fine-mode (FMF). The merged results for aerosol size indicate that aerosols should be smaller over land but larger over oceans than suggested by the modeling background.

A major advance in MACv2 is an aerosol absorption attribution to smaller (fine-mode) and larger (coarse-mode) aerosol sizes. Considering that the spectral slope of aerosol absorption is more negative from the UV to the VIS (spectral region) for dust (and for organics) compared to soot (but similar in slope to BC from the VIS to the nIR), a simple parameterization has been defined. This parameterization applies spectral absorption information of sky-photometer samples and information on the fine-mode AOD fraction. The resulting absorption separation into the two size-modes is presented in Figure A2. This general parameterization, however, leaves too much fine-mode absorption over desert regions and too much dust over biomass regions. This is largely caused by the independent merging of AOD and AAOD for each of the two sizes-modes. Since there is more confidence in mode attributions for AOD (e.g. better observational statistics and coverage), three additional constraints to re-distribute the AAOD were introduced: (1) the coarse-mode AOD over continents has to be dust, (2) dust contributes stronger in larger coarse mode AOD cases over tropical oceans and (3) dust has a mid-visible composition defining Refractive Index imaginary part (RF,imag) value of 0.001 (based on size vs RF,imag matches to coarse mode absorption data over the Sahara). As a result, see Figure A3, AAOD dust contributions in the tropics are increased, at the expense of the fine-mode AAOD and fine-mode AAOD is increased over wildfire regions.

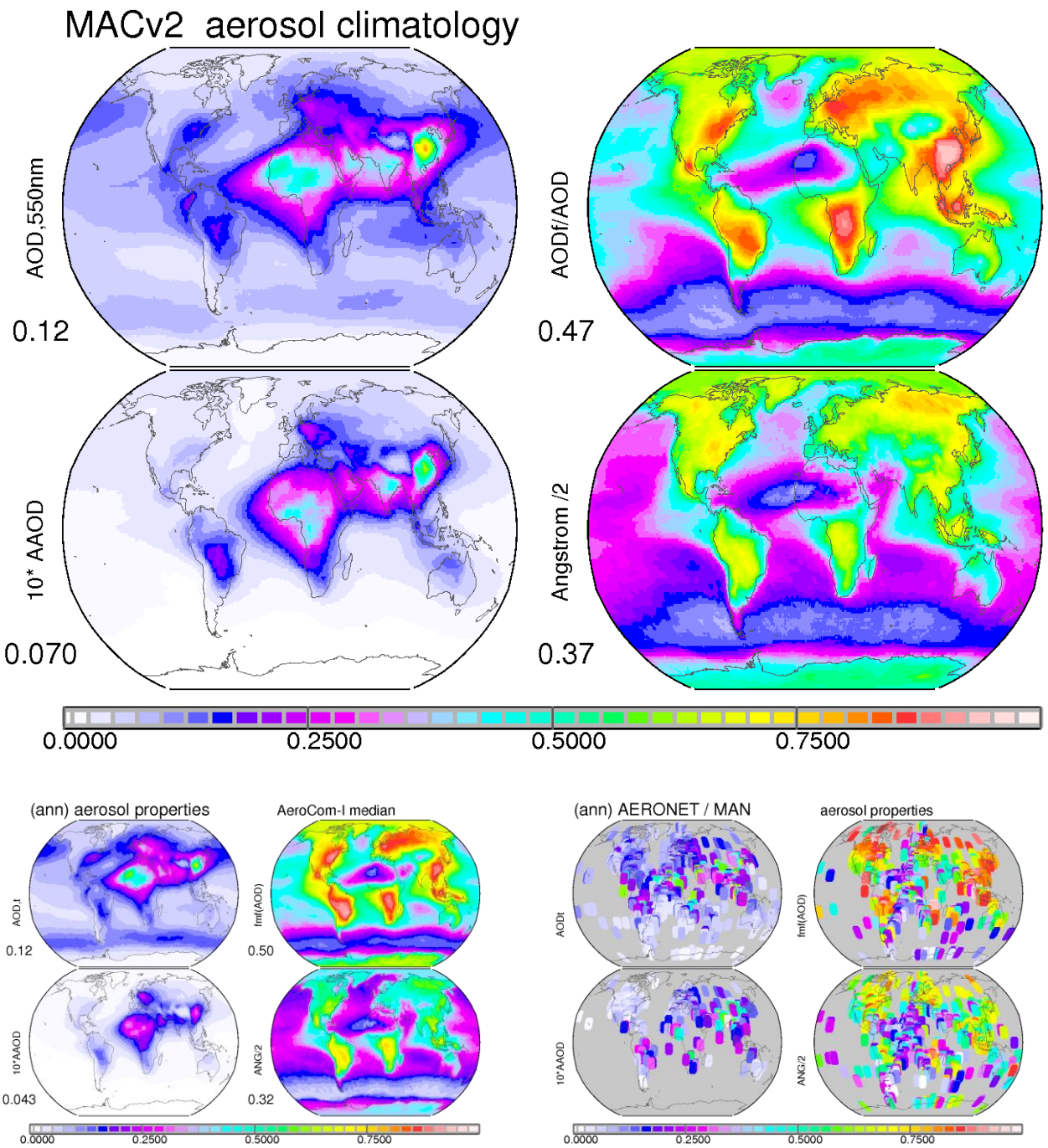

Figure A1 Aerosol properties for column amount (AOD at 550nm, upper left panels), column absorption (AAOD at 550nm, lower left panels) and aerosol size (AOD fine-mode fraction, upper right panels and Angstrom parameter, lower right panels). The upper part displays the annual fields of the MACv2 climatology and the lower panels display the contributing data from sun-photometer observations (AERONET/MAN) and bottom-up global modeling (AeroCom 1 median).

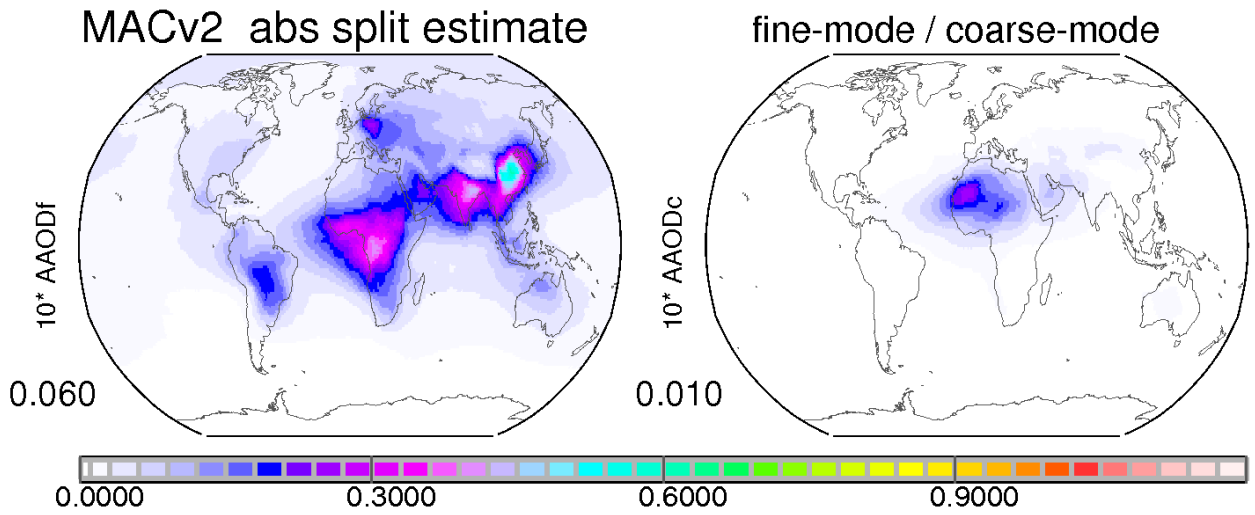

Figure A2. Estimate for aerosol absorption attribution between fine-mode and coarse-mode sizes in MACv2 using AERONET data on RF,imag spectral (440, 670, 1020nm) variability and fine-mode AOD fraction: fmF,AAOD = fmF,AOD**([0.20 +0.25*(1-fmF,AOD)**2]* [AAE_440_670/AAE_670_1020 /2] **4) where AAE is the absorption spectral slope (Absorption Angstrom Exponent) between two different solar wavelength pairs ('440nm and 670nm' and '670nm and 1020nm')

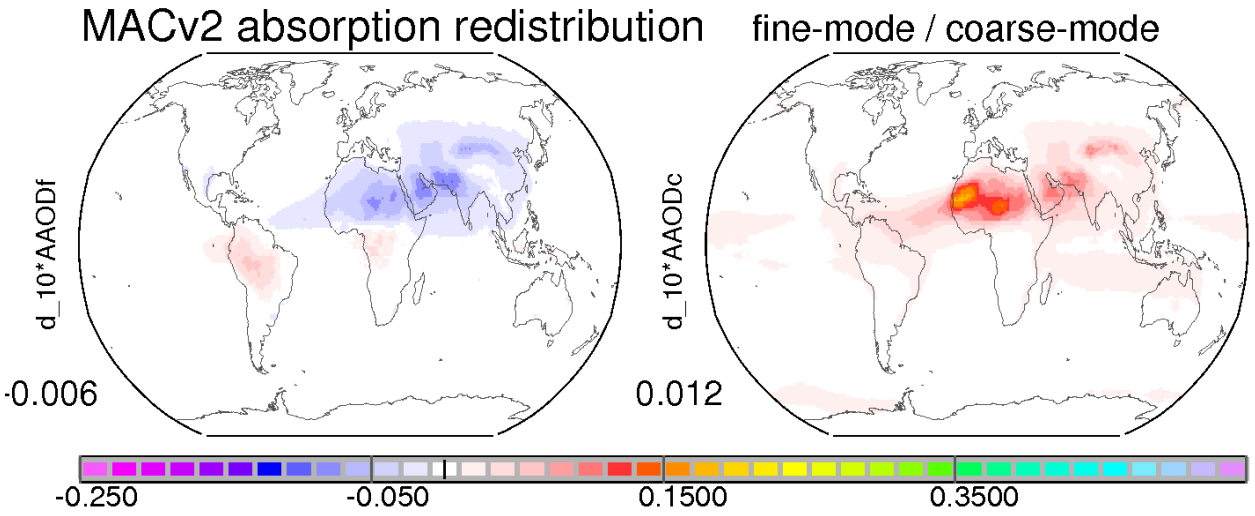

Figure A3. Absorption adjustment for fine-mode (left) and coarse-mode (right) in MACv2. It considers (with the assumption that the coarse/fine AOD split is correct) that (1) dust is present according to the coarse-mode AOD over continents, (2) over tropical oceans most of larger coarse mode AOD are attributed to dust and (3) the dust absorption potential is set to a relatively low absorption values in the mid-visible (RF,imag, 550nm = 0.001 for dust).

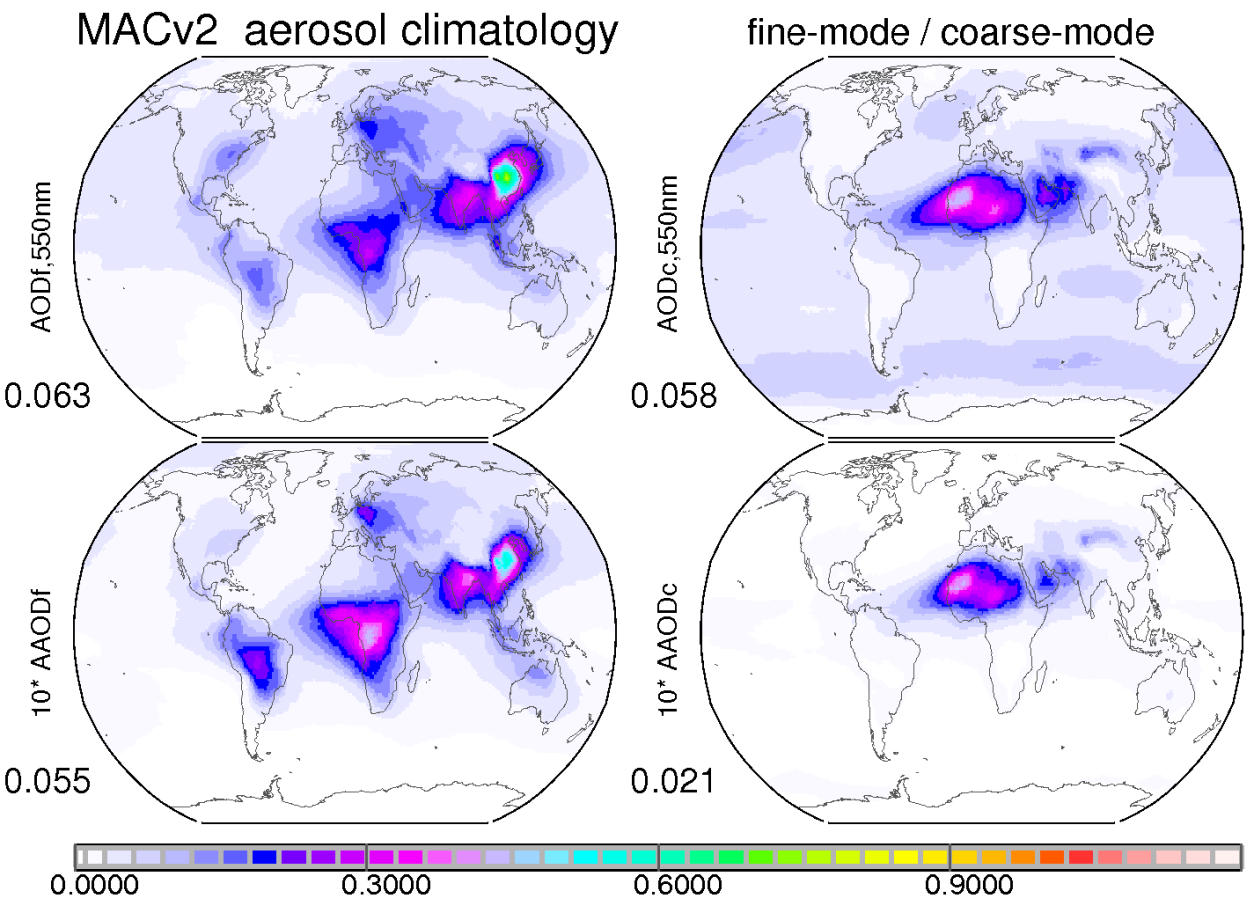

Figure A4 Attribution between fine-mode and coarse-mode sizes in MACv2 for AOD at 550nm (upper row) and for AAOD at 550nm (lower row). Interestingly, dust consumes on a global averages approx. 30% of the mid-visible AAOD – mainly due to its relatively large size and less due to the RF,imag.

Comparisons of annual averages for AOD and AAOD of the fine-mode and for the coarse-mode are presented in Figure A4. A cleaner absorption separation into the two aerosol absorption size-modes is achieved compared to Figure A2. On a global average about 70% of the AAOD are assigned to the fine-mode, while a significant 30% of the AAOD is attributed to dust. As it was assumed that with increased dust AOD also the dust-size increases. Thus, a significant fraction of the coarse mode AAOD is related not to dust composition but to dust size (larger sizes with same absorbing RF,imag value yield lower SSA).

The combined information of AOD and AAOD for both (fine and coarse) size modes permits a separation into component AOD values. The coarse mode AOD separation between dust (reff= 1.5 to 6µm, RF,imag =0.001) and sea-salt (reff=2.5µm, RF,imag = 0.0) is set, as dust contributes to AAOD and seasalt does not. The fine-mode AOD split into three pre-defined components of BC (reff=0.06µm, RF,imag=0.7), OC (reff=0.15µm, RF,imag=.005) and SU (reff=0.2µm, RF,imag=0) requires additional input on the local the fraction of (absorbing) carbon AOD in the fine-mode, which is supplied by bottom-up modeling.

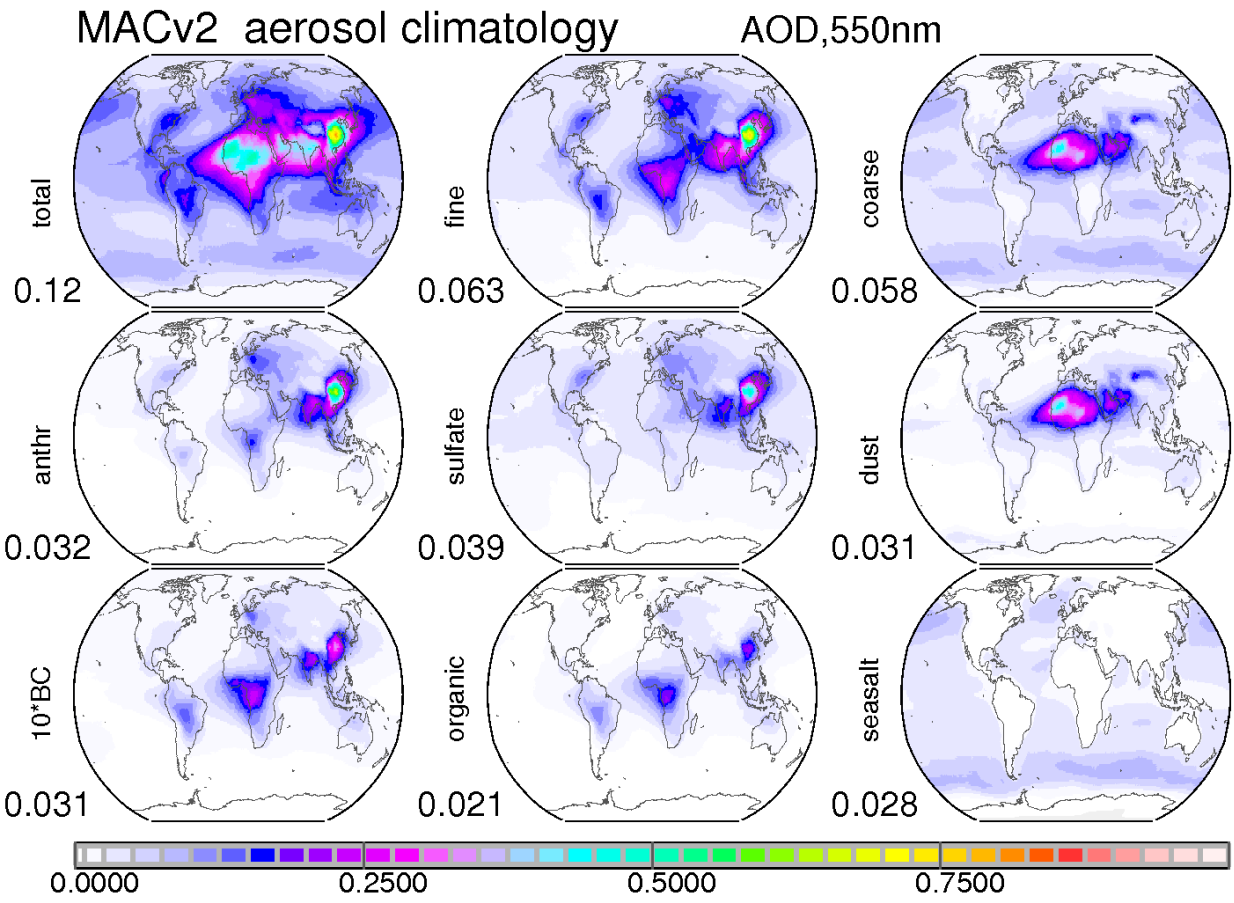

Figure A5. Today's mid-visible aerosol optical depth (AOD at 550nm) of the MACv2 climatology and sub-contributions assigned to aerosol sizes with radii <0.5µm (fine-mode) and to aerosol sizes with radii >0.5µm (coarse mode). The absorption attribution fine-mode and coarse-mode allow to identify component AOD contributions by sulfate (for non-absorbing fine-mode), by organic carbon and black carbon (BC, here enhanced 10 times for better visibility) of the fine-mode AOD and coarse mode components of dust and sea-salt. In addition, also a map for today's anthropogenic (fine-mode) AOD is presented, by applying as scaling factor to the fine-mode AOD based on ratios between today's and pre-industrial fine-mode AOD from bottom-up global modeling.

Annual averages maps of resulting component AOD values for SU, OC, BC SS and DU for today's aerosol properties (year 2005) are presented in comparison to fine-mode, coarse-mode and total AOD in Figure A5. In this figure also a map for today's anthropogenic AOD is given, which is based on the product of the fine-mode AOD (anthropogenic AOD is assumed to have fine-mode AOD contributions) with a scaling factor. This scaling factor defined by the relative increase in the local fine-mode AOD associated with today's emissions compared to fine-mode AOD with pre-industrial emissions and is supplied by simulations with bottom-up modeling. This resulting map for the anthropogenic AOD map is approximated in the simplified MACv2-SP plume approach.

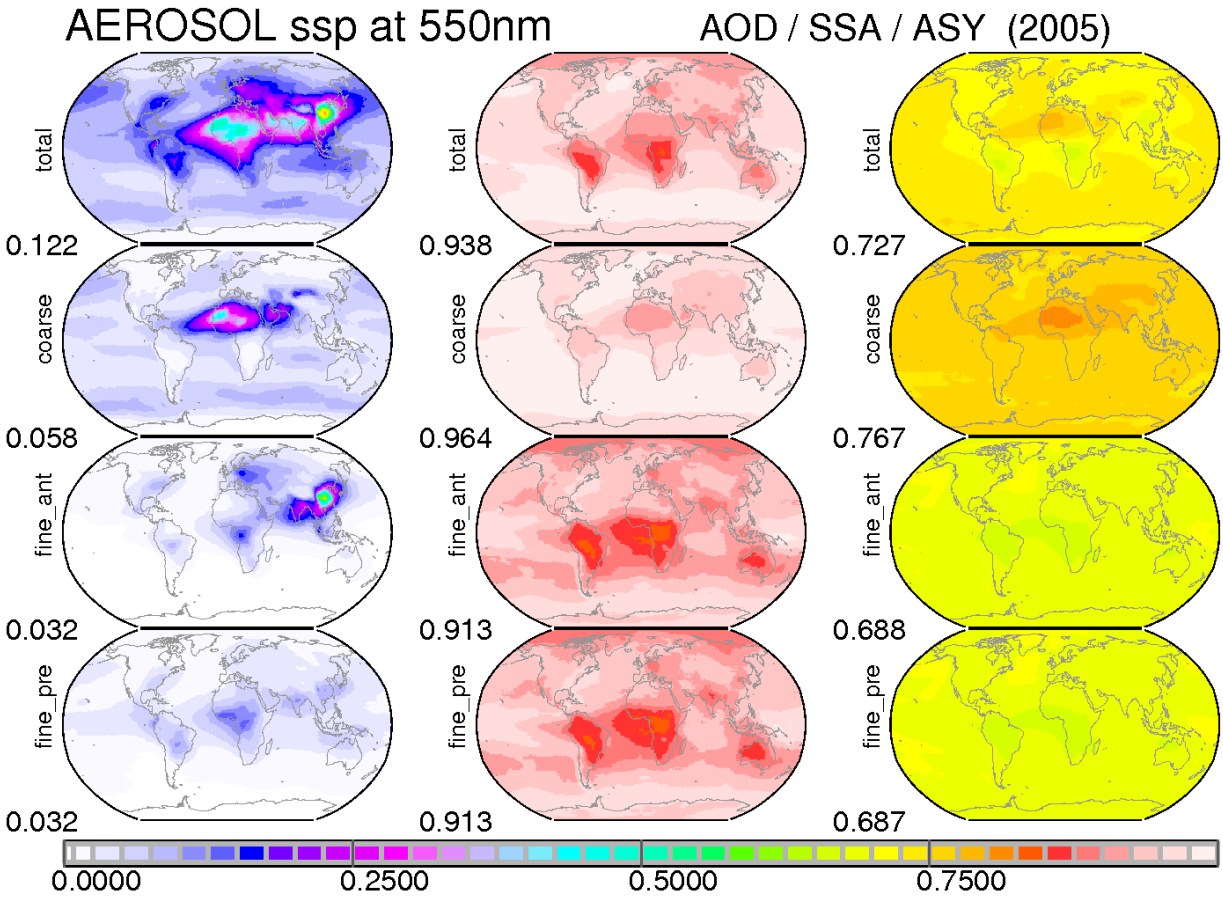

Figure A6. Annual averages of mid-visible aerosol single scattering properties (aerosol optical depth: AOD, single scattering albedo: SSA, asymmetry-factor: ASY) of MACv2. The left column displays AOD at 550nm, the center column SSA at 550nm and the right column ASY at 550nm. Results are presented for today's (year 2005) total aerosol (row 1), coarse-mode aerosol (row 2), today's anthropogenic aerosol (row 3) and for assumed pre-industrial (year 1850) fine-mode (row 4).

Based on pre-defined properties for the aerosol components (BC, OC, SU, DU and SS) and their relative AOD contributions now the single scattering properties can be determined as they are needed in broadband radiative transfer simulations: the aerosol optical depth (AOD, 'how much is there?'), the single scattering albedo (SSA, 'how much of the attenuation is scattered?') and the asymmetry-factor (ASY, 'what is angular distribution of scattering events?'). Mid-visible properties for total aerosol, coarse-mode aerosol as well as anthropogenic and pre-industrial fine-mode aerosol are presented in Figure A6. Note that at 550nm the fine-mode absorption potential (SSA=0.913) is much larger than that for the coarse mode (SSA=0.964). The larger coarse mode size with its tendency towards a stronger forward scattering yields a larger value (ASY=0.767) than the fine-mode (0.688). The pre-industrial fine-mode aerosol has the same SSA and ASY values as the later added anthropogenic aerosol. In future updates of the climatology the consideration of compositional changes to added anthropogenic aerosol will be entertained.

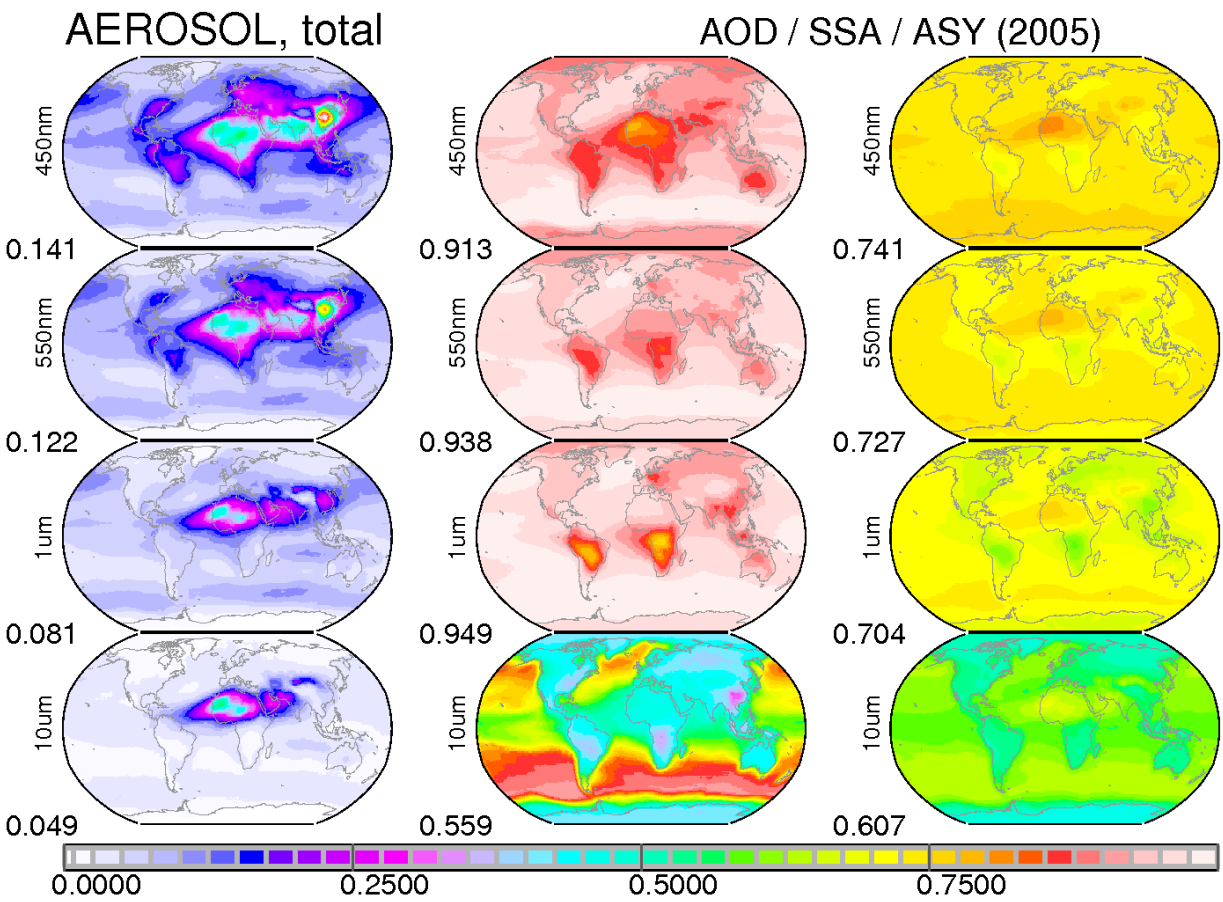

Figure A7. Annual averages of single scattering properties (aerosol optical depth: AOD, single scattering albedo: SSA, asymmetry-factor: ASY) for today's total aerosol of MACv2 at four different wavelengths: .45 (UV), .55 (VIS), 1 (near-IR) and 10um (far-IR). Presented are atmospheric column averages for AOD (column 1), SSA (column2) and ASY (column 2). Values below the labels present global averages.

When defining the different aerosol components, also their refractive indices at wavelengths other than the mid-visible were assigned in order to be able to satisfy the spectrally varying input for the three aerosol single scattering properties (AOD, SSA and ASY).

The resulting properties at selected wavelengths in the UV (450nm), mid-visible (550nm), near-IR (1.0µm) and far-IR (10µm) are presented for total aerosol in Figure A7 and for coarse-mode aerosol in Figure A8. The spectral variability for the total AOD is mainly caused by the fine-mode. Compared to the mid-visible AOD, fine-mode contributions are larger in the UV, weaker in the near-IR and almost gone in the far-IR. The single scattering albedo for total aerosol shows relative low values in the UV over the Sahara due to stronger absorption by dust and in the near-IR over both southern continents - as absorption becomes more effective than scattering when already low ratios between (wild-fire fine-mode aerosol) size and (near-IR) wavelength get even smaller. Dust AOD is almost invariant. In the far-IR only smaller dust (as assigned to remote regions) degrades in their AOD, while for larger dust sizes (near sources as in the central Sahara) even display an AOD increase.

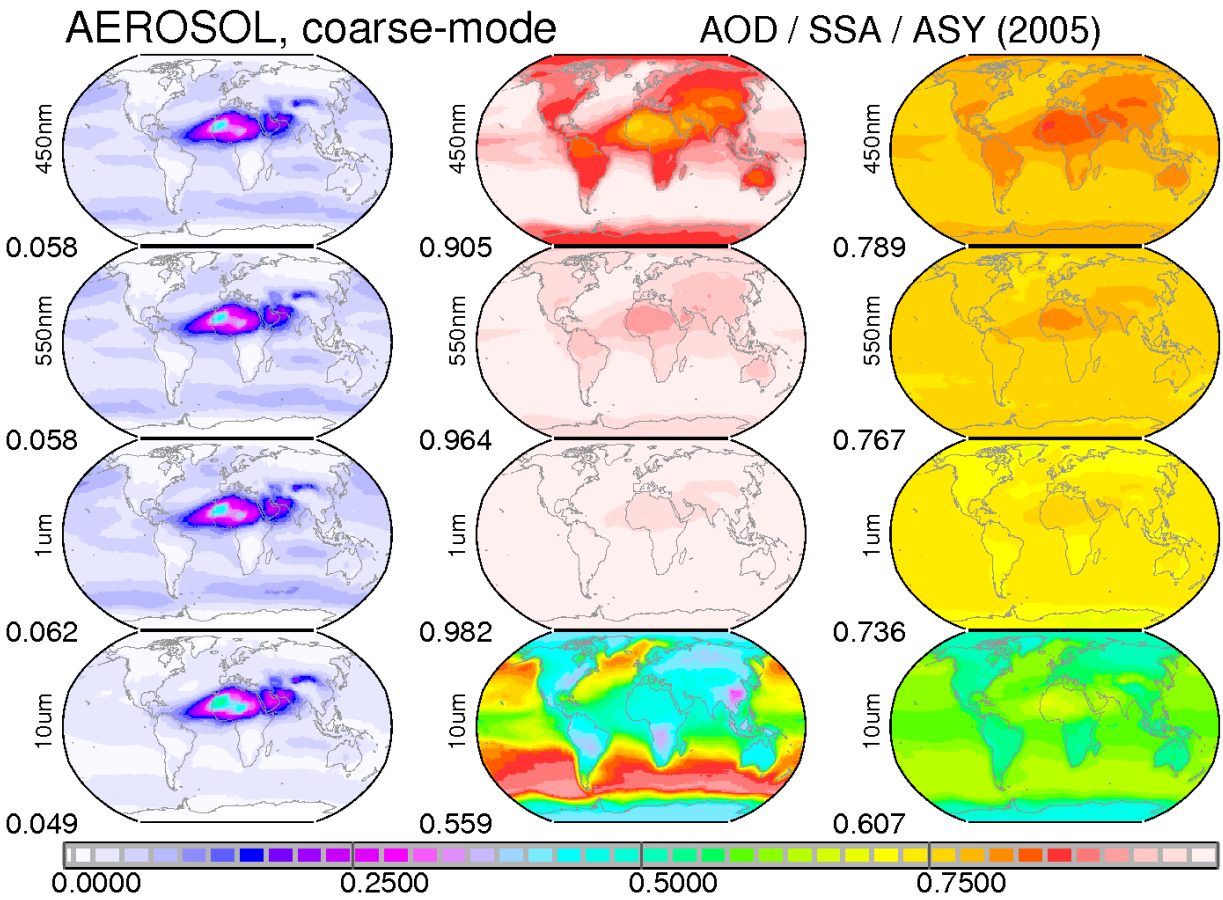

Figure A8. Annual averages of single scattering properties (aerosol optical depth: AOD, single scattering albedo: SSA, asymmetry-factor: ASY) for coarse-mode aerosol of MACv2 at four different wavelengths: .45 (UV), .55 (VIS), 1 (near-IR) and 10um (far-IR). Presented are atmospheric column averages for AOD (column 1), SSA (column2) and ASY (column 2). Values below the labels present global averages.

Similarly, spectral properties for anthropogenic aerosol (its SSA and ASY are also that of the fine-mode, thus also valid for the pre-industrial fine-mode) are presented in Figure A9 at selected wavelengths in the UV (450nm), mid-visible (550nm) and near-IR (1.0um and 1.6um). The absorption (AAOD) at 450nm is already 30% larger than the mid-visible AOD (simply due to fine-mode size). And absorption increase will even further accelerate towards smaller wavelengths, when stronger organic absorption adds to contribute. In contrast, towards the near-IR the fine-mode absorption drops sharply and it is at (a wavelength of) 1.0µm only 1/3 of the mid-visible absorption.

Aside from the aerosol single scattering properties also the aerosol microphysical properties are of interest, that is, if they can be derived from the optical properties. Most important for aerosol indirect effects are aerosol concentration at the cloud base, more specific only those concentrations that are large enough (larger than a 'critical radius') to potentially develop into cloud droplets, so called cloud condensation nuclei (CCN). Considering the local aerosol composition of the climatology (sulfate and sea-salt require a lower radius threshold than organics, while soot and dust are unlikely to contribute) the critical radii for different super-saturations were calculated and are presented in Figure A10. For super-

saturations of 0.2, 0.1, 0.07 and 0.05% the critical radii are at .09, .14, .17 and .20µm, respectively. Based on this range of super-saturations all coarse-mode aerosol particles are CCN but only a fraction of the fine-mode aerosol particles qualifies. By assuming a log-normal size-distribution with a prescribed distribution width (std. dev. of 1.7) and employing complementary size information of Angstrom and FMF, a size-distribution for the fine-mode is constructed and all fine-mode particles larger than the critical radius are considered CCN. In a last step for each mode its AOD along with the scaled information on its relative vertical distribution (from bottom-up modeling or alternately from CALIPSO lidar data) is applied at an altitude near 1km (the approximate cloud-base height of low altitude water clouds) to yield CCN estimates.

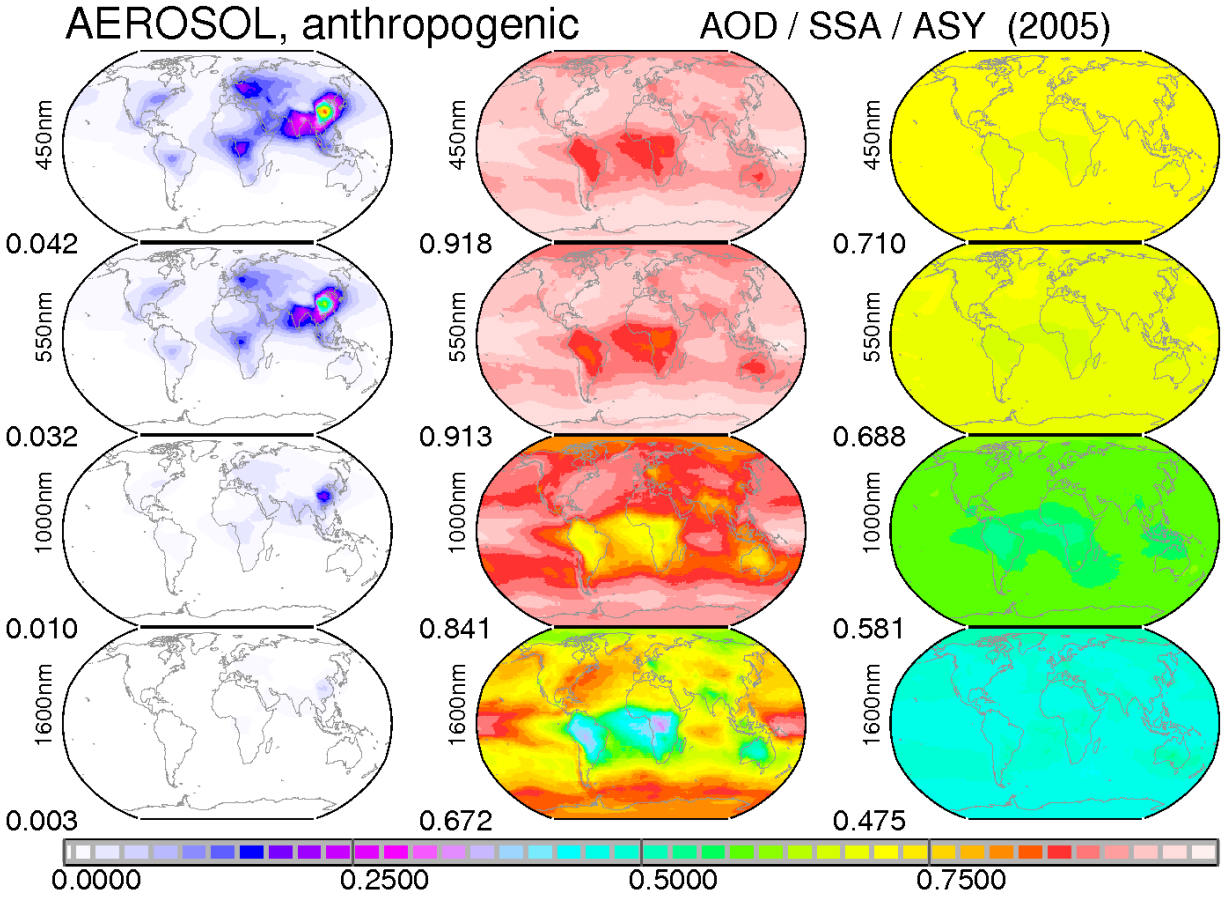

Figure A9. Annual averages of single scattering properties (aerosol optical depth: AOD, single scattering albedo: SSA, asymmetry-factor: ASY) for today's anthropogenic aerosol of MACv2 at four solar wavelengths: .45 (UV), .55 (VIS), 1.0 and 1.6µm (near-IR). Presented are atmospheric column averages for AOD (column 1), SSA (column2) and ASY (column 2). Values below the labels present global averages.

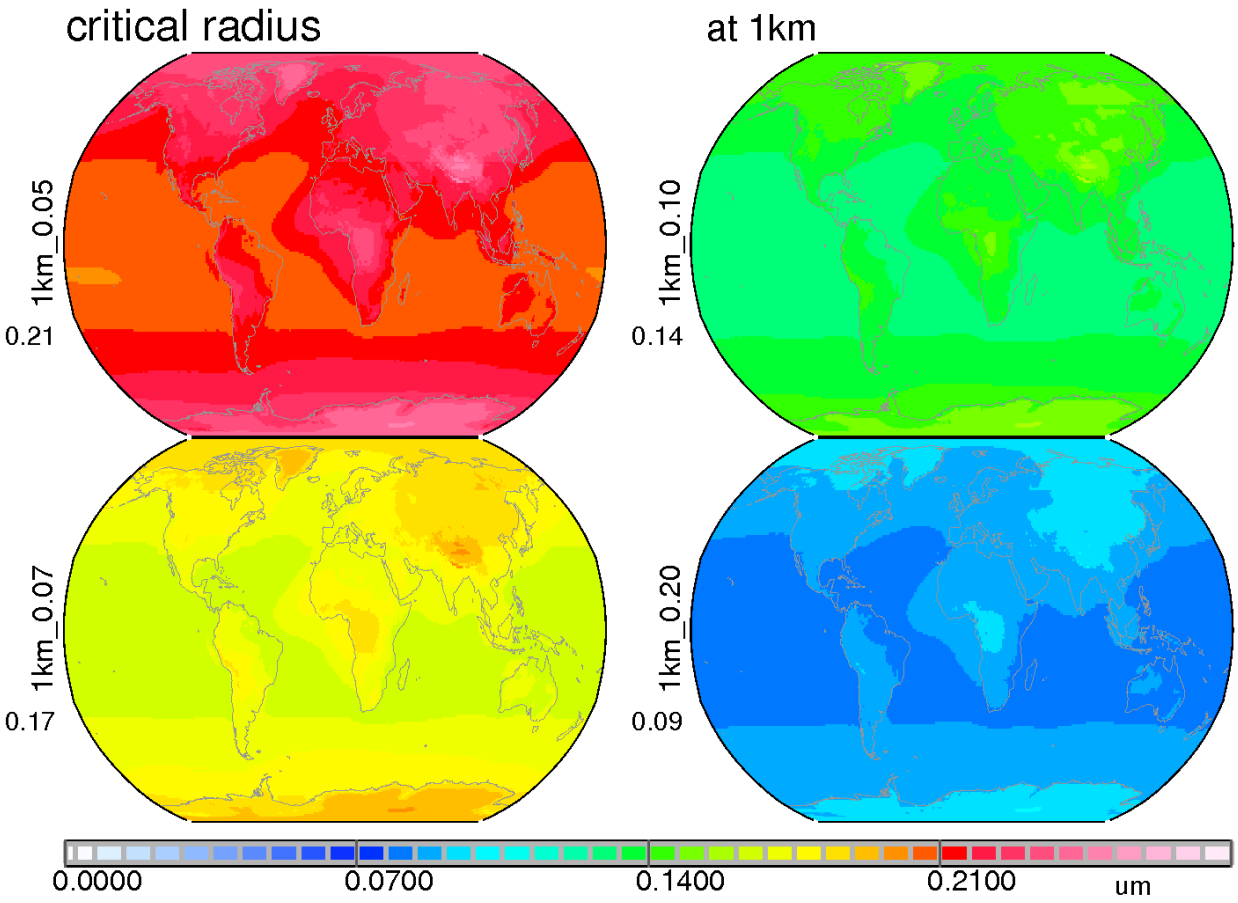

Figure A10. Spatial distributions of critical fine-mode radii at 1km altitude as function of 4 different super-saturations (0.05%, 0.07%, 0.1 and 0.2%). All aerosol particles larger in size are considered cloud condensation nuclei (CCN). Values below the labels present global averages.

For the pre-selected four super-saturations of 0.05, 0.07, 0.10 and 0.20% CCN estimate at 1km altitude CCN concentrations are estimated for anthropogenic added aerosol in Figure A11 and for natural (coarse and pre-industrial fine) aerosol in Figure A12. It is much more difficult to offer CCN, when (water vapor) super-saturations are weak. Anthropogenic CCN are often less than natural CCN in very remote regions und usually anthropogenic CCN concentration are larger, actually larger by many factors over regions with stronger pollution. Finally, in a last step the anthropogenic CCN increase is converted into a cloud-droplet concentrations (CDNC) increase assuming a logarithmic relationship. Such a relationship is justified, as same additions of CCN yield stronger CDNC increases at CCN poor than under CCN rich background conditions.

Local annual averages for CDNC changes for an assumed super-saturation of 0.10% are presented in Figure A13. Assuming the cloud liquid water is not modified, the cloud droplet radius is decreased (as more nuclei compete for the available cloud water) and along with it the cloud optical depth is increased.

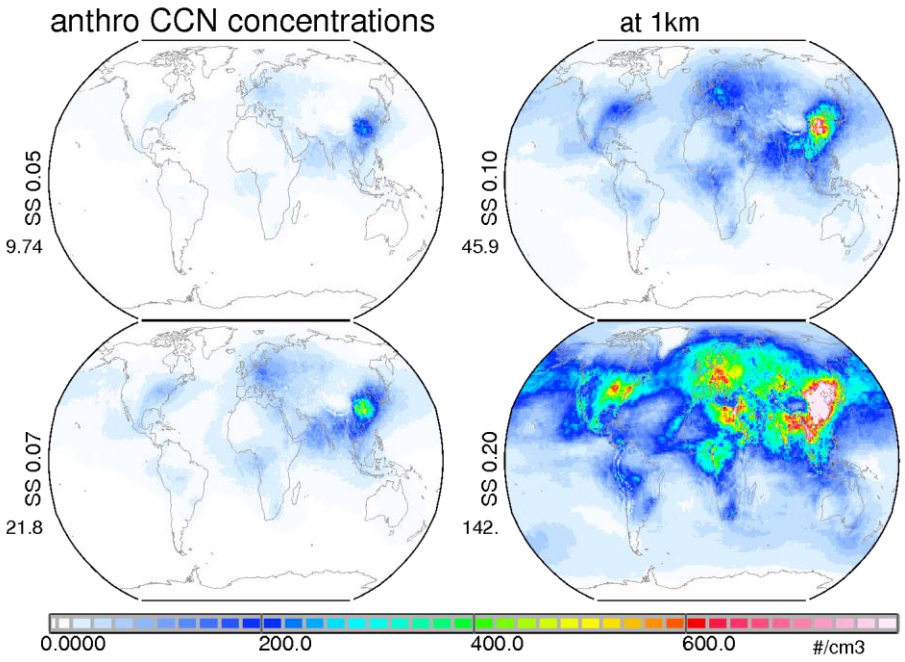

Figure A11. Today's ('year 2005') anthropogenic CCN at 1km altitude as function of four different super-saturations (0.05%, 0.07%, 0.10 and 0.20%) of MACv2.

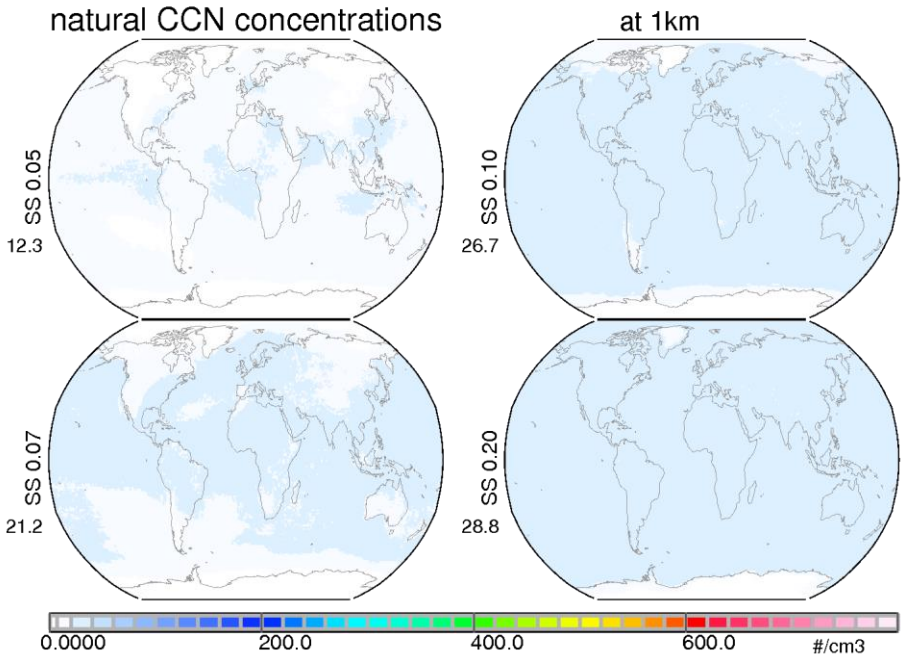

Figure A12. Natural CCN at 1km altitude as function of four different super-saturations (0.05%, 0.07%, 0.10 and 0.20%) of MACv2.

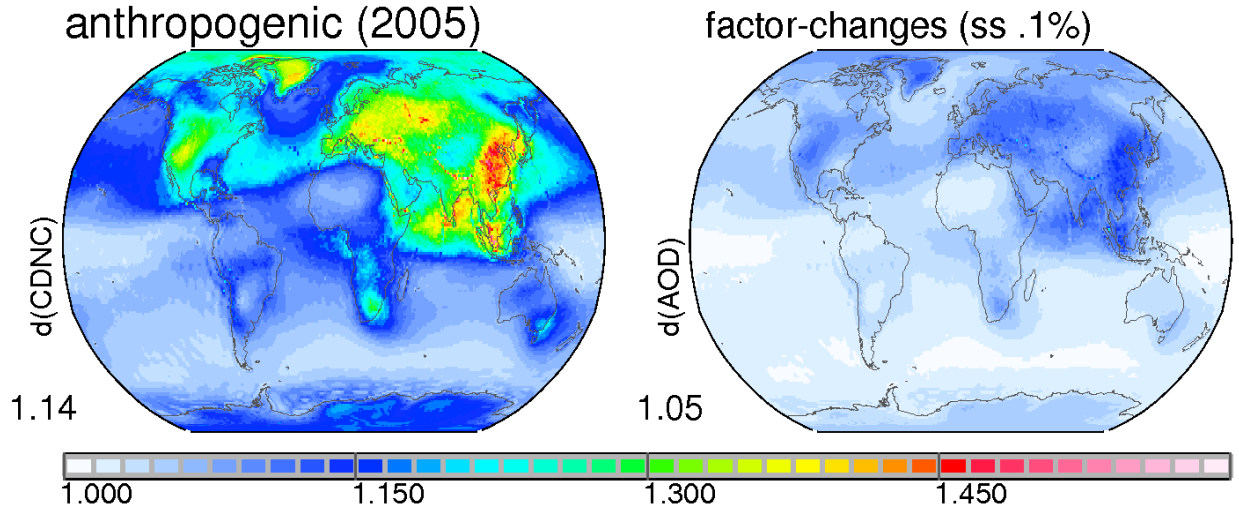

Figure A13. Annual average increases to CDNC (left panel) and increases to low (water) cloud optical depth (right panel) for 0.1% super-saturation.

Annual averages for (low altitude water) cloud optical depth increases for an assumed super-saturation of 0.10% are also shown in Figure A13. Resulting increases to the planetary albedo will be termed aerosol indirect effect.

Finally, to make this climatology for aerosol optical properties and also derived aerosol compositional and microphysical properties more useful three additional external data from bottom-up modeling are adopted for scaling: (1) the fraction of today's fine-mode AOD that is anthropogenic, (2) the temporal change of this anthropogenic fraction, (3) the AOD vertical distribution for both size-modes (see also Kinne et al., 2013) and now in MACv2 also the component based carbon fraction for fine-mode AOD. The first two supplementary data sets are needed quantify today's aerosol climate impact and its change over time (past and future), while the third supplementary data is needed to address the dust IR radiative effect and impacts in the context of clouds, as the relative altitude between aerosol and clouds matters. Resulting MACv2 data are accessible via
ftp: ftp-projects.zmaw.de/aerocom/climatology/MACv2_2017.

Finally, it also should be mentioned that in off-line simulations of aerosol radiative effects and aerosol forcing additional external global data-sets are used: (1) cloud properties of ISCCP (e.g. high, mid and low altitude cloud fractions and cloud optical depth), (2) surface properties including MODIS land surface albedo, NOAA's ice and snow cover and GISS surface temperature and (3) atmospheric profiles of AGFL's standard atmospheres.

Appendix B **Further simplifications in MACv2-SP**

For further simplifications, mainly to serve as aerosol seed in RFMIP simulations a derivation of the MACv2 aerosol climatology, MACv2-SP (SP for single plumes) has been developed in parallel (Stevens et al., 2016). With a focus on anthropogenic aerosol impact and its change over time, today's anthropogenic AOD map of the gridded MACv2 has been approximated by the sum of nine analytical plumes around nine aerosol sources as illustrated in Figure B1.

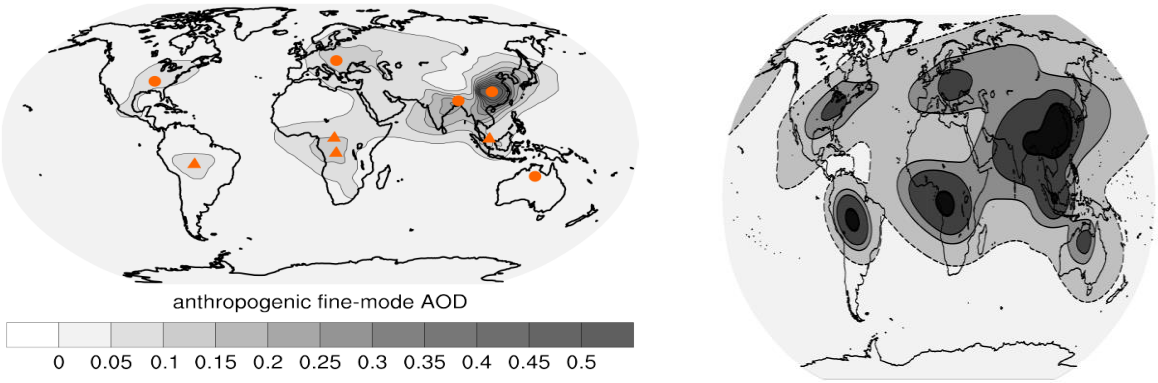

Figure B1 Global distributions of the nine source regions (five industrial regions: red spheres and four wild-fire regions, red triangles), whose plumes can reproduce the anthropogenic aerosol monthly maps of MACv2 for today's conditions (annual averages of MACv2 are presented as background in the left panel) within about 20%. The right panel illustrates the concept of overlying plumes to represent the anthropogenic AOD maps for the month of September, when wild-fires over the southern continents have larger contributions.

Such a plume representation has the advantage that aspects of transport and processing away from sources are considered so that temporal change anthropogenic (sulfate and nitrate) emissions can be easily implemented by source scaling.

Another simplification aspect of the MACv2-SP approach is that in order to quantify the (for climate impacts important indirect effect) of anthropogenic aerosol on cloud water droplet concentrations (with subsequent increases to water cloud optical depth and planetary albedo - also termed Twomey effect), the complex process (involving aerosol number, super-saturation, aerosol composition, critical radius, CCN to CDNC relationships) is side-stepped. This is done by applying satellite sensors data based (thus 'observational') relationships of proxies for aerosol number (fine-mode AOD) and cloud-droplet number. The rational is that the detected cloud droplet number at the cloud-top represents also the number at cloud-base (assuming adiabatic conditions) and that the (column property) of the fine-mode AOD is usually strongest at water cloud altitudes. Apparently limiting aspects that (1) monthly averages of associations between AODf and CDNC at 1x1 deg lon/lat resolution are used, (2) that only oceanic data are used (where retrievals are more reliable) and (3) spatial context is rendered to help statistics are set aside and the resulting logarithmic relationship is presented in Figure B2.

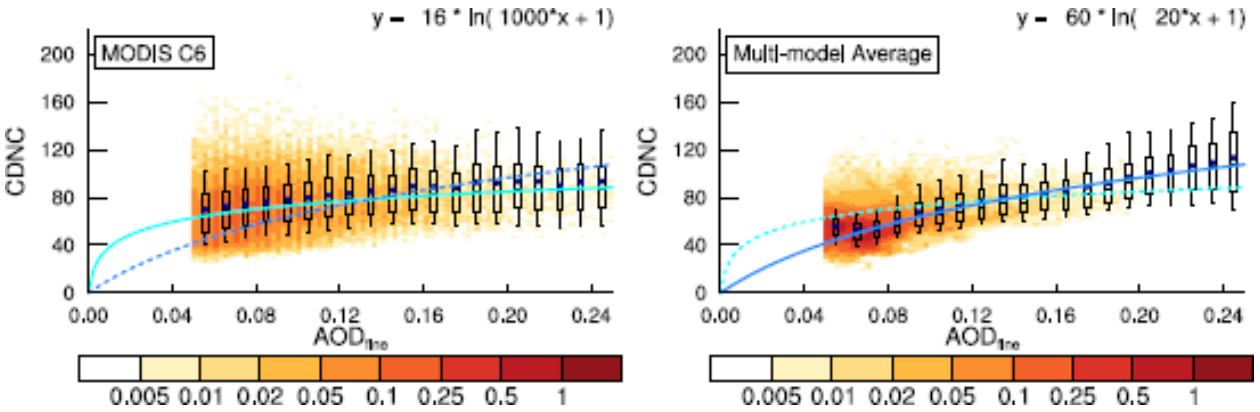

Figure B2. Average relationships between fine-mode AOD (AODf) and water cloud droplet number concentrations (CDNC) as observed with satellite remote sensing over oceans (MODIS, left panel) and as suggested by global modeling at the same locations (AeroCom ensemble, right panel). Note that models suggest a much stronger CDNC change by changes in (fine-mode) anthropogenic aerosol. To determine the indirect effect of anthropogenic aerosol the average relationship from (MODIS) satellite observations (CDNC =16*ln(1000*AODf+1) is applied twice (once for total AODf and once for pre-industrial AODf) to determine the anthropogenic change to CDNC .

The presented 'observational' joint histogram is based on filtered data (1) minimum AODf of 0.05, (2) only CDNC data overcast conditions and near overhead viewing and (3) only oceanic data. The final relationship is a fitted line through the median values for investigated statistics within individual AODf-value bins. The relationship CDNC ~ ln(1000*AODf) derived from MODIS-v6 data is quite similar when using alternate satellite data (e.g. MODIS-v5, or ATSR). [In that context, CDNC data provisions for MODIS-v6 by J. Rausch, for MODIS-v5 by D. Grosvenor and for ATSR by M. Christensen and also the data-processing by J. Muesse are acknowledged].

Figure B2 also shows the equivalent joint histogram when data of global models (from AeroCom indirect experiment output) are sampled at the same locations as the satellite data. The median fitted relationship of the models, however, is much steeper. This suggests that the Twomey effect is overestimated in many global models.

To determine an CDNC increase due to extra anthropogenic aerosol the 'observational' relationship, CDNC ~ ln(1000*AODf), is applied twice: (1) once for the total AODf and (2) once for reference (e.g. pre-industrial) AODf. Hereby the needed AODf reference field in MACv2-SP is prescribed by a constant AODf=0.02 background combined with source strengths at pre-industrial conditions (based on historic emission data for sulfate nitrate by S. Smith).

This simple 'observational' relationship between AODf and CDNC was also applied in the MACv2 climatology to examine to what degree the approach simplifications yield Twomey aerosol effect biases in terms of strength and pattern. Comparisons for the annual indirect forcing at today's conditions (and not just limited to ocean regions of the observations) between the fit approach and a more complex treatment of MACv2 (via CCN) are presented in Figure B3.

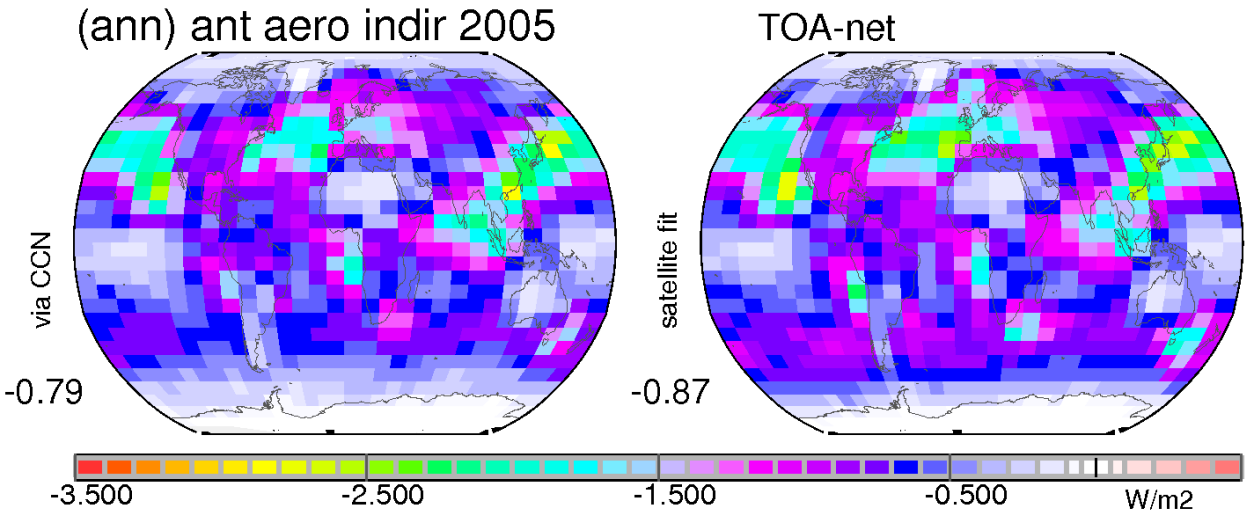

Figure B3: A comparison of annual indirect radiative effects by today's (year 2005) anthropogenic aerosol between a more detailed method (left panel, using fine-mode particle concentrations, composition (via kappa values) and assumed super-saturations (0.1%) to determine CCN and eventually CDNC changes) and a simplified methods (right panel, based on a satellite observed relationship between AODf and CDNC) to link CDNC changes directly to anthropogenic AOD.

Surprisingly, the two forcing patterns are quite similar, which is probably also helped that other aspects (sun-elevation, available sun-light, darkness of background, single low altitude cloud frequency) are influential for the indirect aerosol impact. Still, through the nice reproduction of the spatial indirect aerosol forcing patterns, the simple approach demonstrated its merit, also to serve as constraint for the Twomey effect in RFMIP simulations.

Appendix C **Aerosol radiative effects of MACv2**

This section contains some supplementary figures on instantaneous aerosol radiative effects from radiative transfer simulations with the MACv2 aerosol climatology.

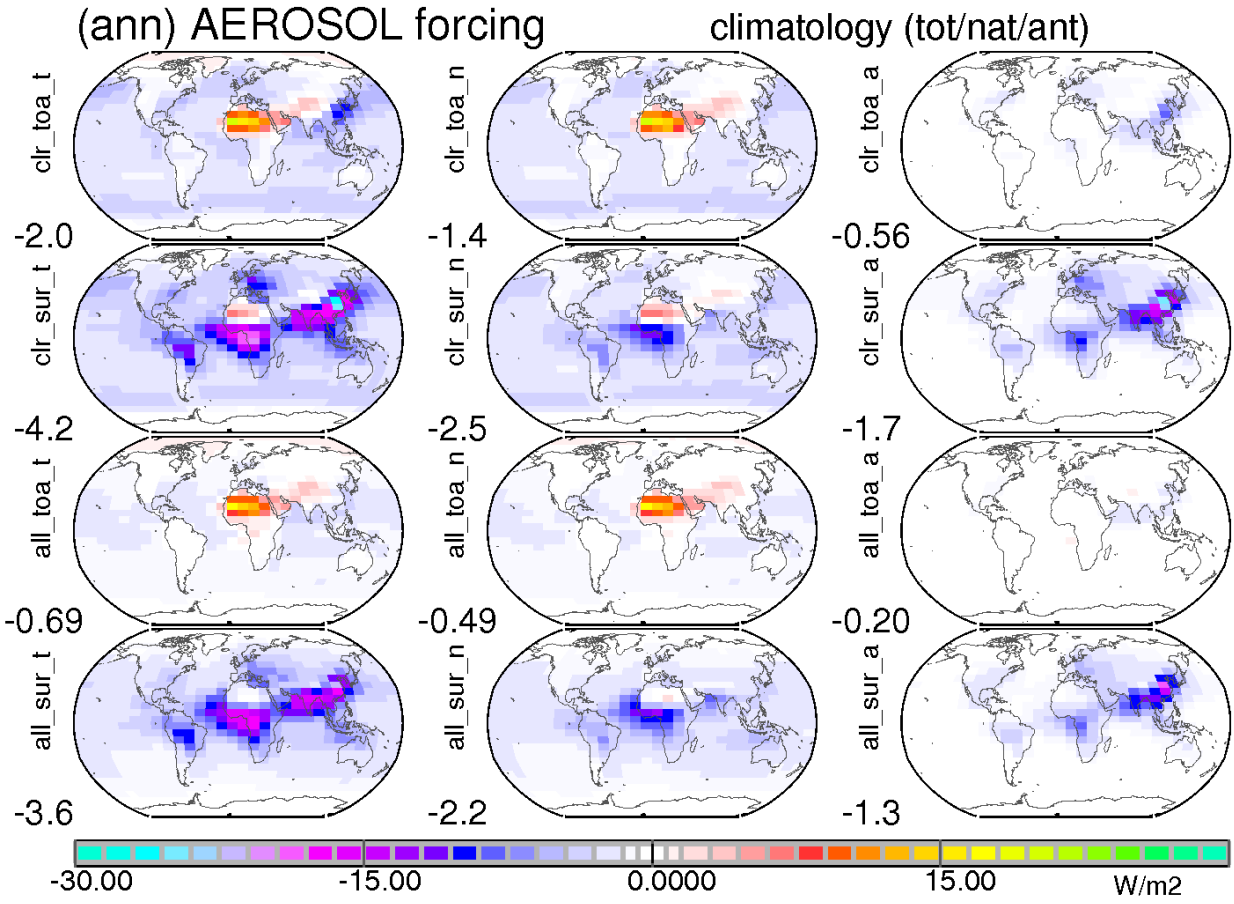

Figure C1: Tropospheric annual aerosol direct radiative effects by applying the MACv2 climatology. The top two rows give spatial distributions of the aerosol radiative effects at cloud free conditions and the bottom two rows include ISCCP clouds for all-sky simulations. Rows 1 and 3 display the effects on radiative net-fluxes at ToA, while rows 2 and 4 show the effects on radiative net-fluxes at the surface. Column 1 show results for today's total aerosol, column2 shows results for natural (or pre-industrial) aerosol and column 3 shows results for today's anthropogenic aerosol. The 3rd panel in the 3rd row represents the direct forcing (ToA, all-sky) for anthropogenic aerosol, which is very small compared to all other presented aerosol effects. Values below labels show global averages.

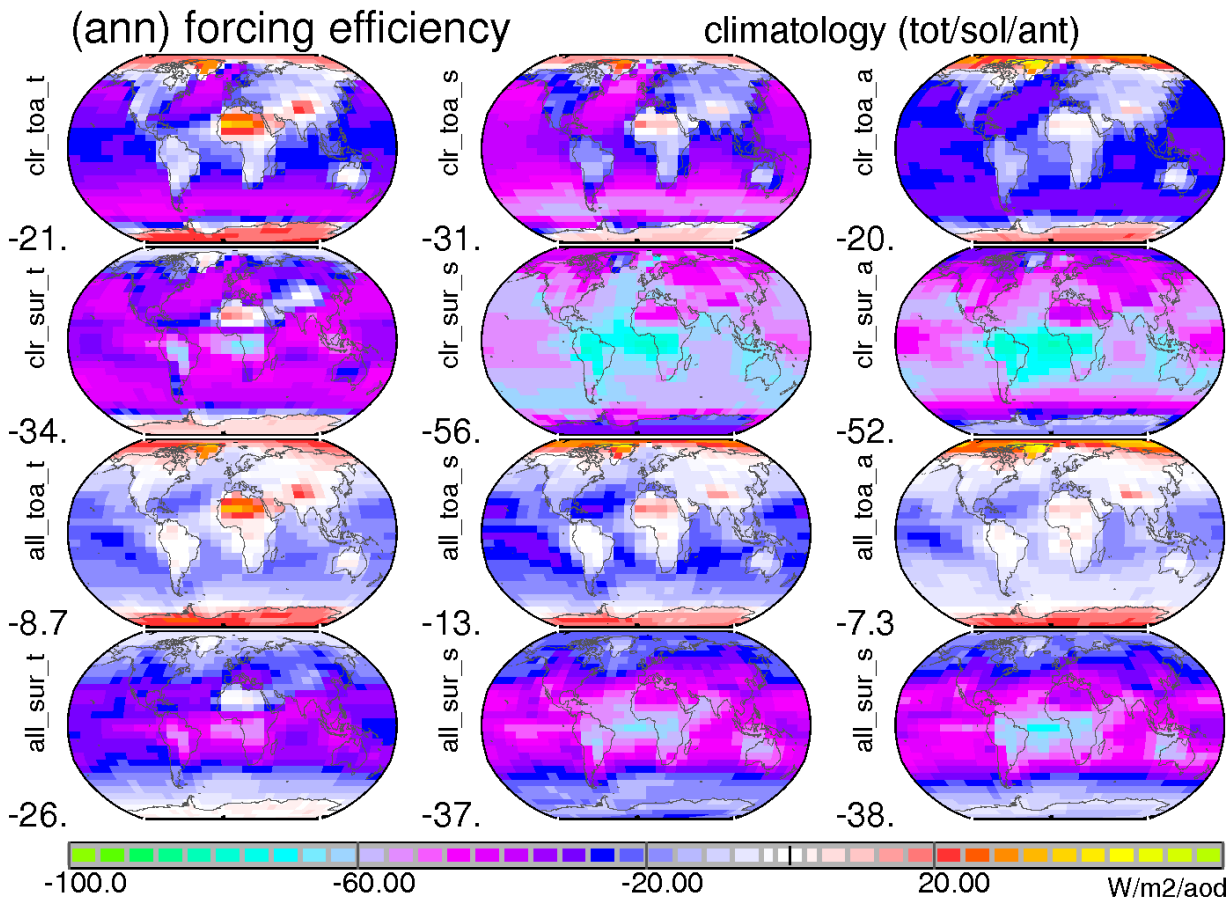

Figure C2: Tropospheric annual aerosol direct radiative effects efficiency per unit AOD by applying the MACv2 climatology. The top two rows give spatial distributions of the aerosol radiative effects at cloud free conditions and the bottom two rows include ISCCP clouds for all-sky simulations. Rows 1 and 3 display the effects on radiative net-fluxes at ToA, while rows 2 and 4 show the effects on radiative net-fluxes at the surface. Column 1 show results for today's total aerosol, column2 shows results today's solar only impact for the total aerosol and column 3 shows results for today's anthropogenic aerosol. The 3rd panel in the 3rd row represents the direct forcing (ToA, all-sky) for anthropogenic aerosol.

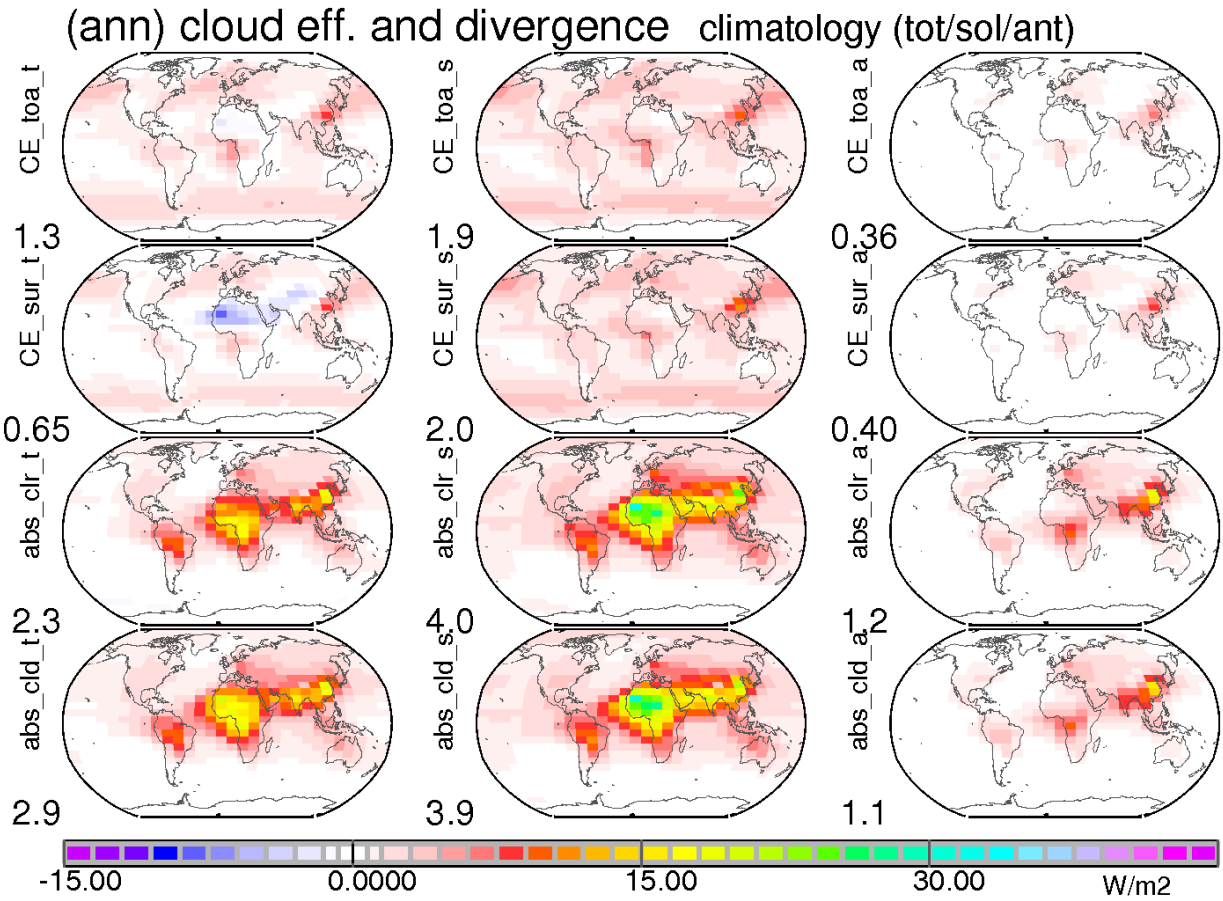

Figure C3: Annual impacts of (ISCCP) clouds on aerosol radiative effects net-fluxes at TOA (row 1) and net-fluxes at the surface (row 2) and annual aerosol direct radiative effects on the atmosphere at clear-sky (rows 3) and all-sky conditions (row 4) by applying the MACv2 aerosol climatology. Column 1 displays results for the entire solar and infrared spectral regions, column2 shows results for only the solar spectral regions and column 3 presents contributions for today's anthropogenic aerosol.

Appendix D **Historic source variability for MACv2-SP**

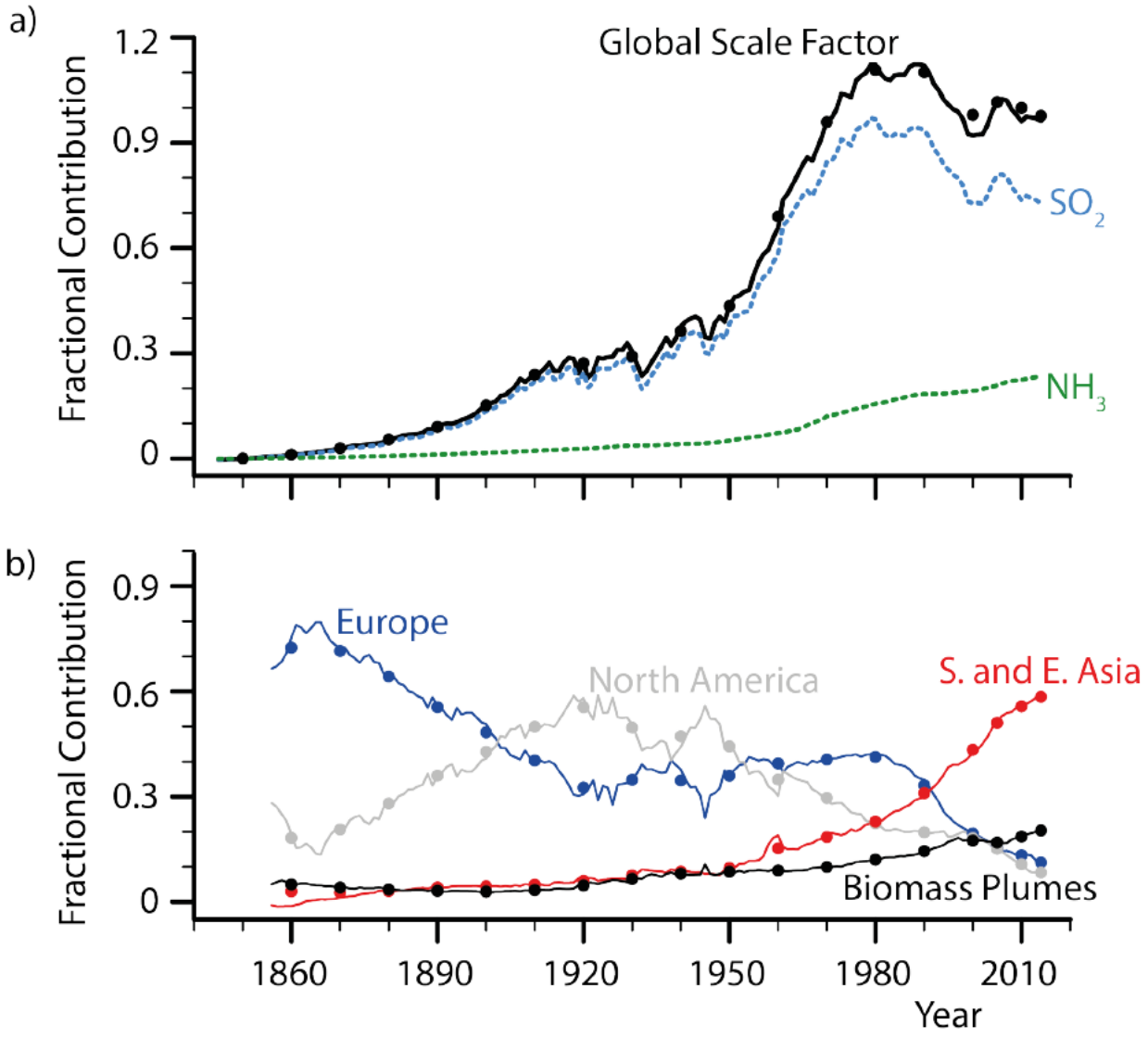

Figure D1. Historic emission data changes (from S. Smith) for sulfate and nitrate which are applied with weight factors of 0.65 for sulfate and 0.35 for nitrate to determine the source strength of the plumes in MACv2-SP. The upper panel global average, while the lower panel shows relative contributions from different source regions.